

LUND UNIVERSITY

MASTER'S THESIS

Patient-Specific 3D Printed Guides for Corrective Osteotomies of Malunited Radius

Author:

Carolin SKYBORN
MSc Engineering Physics

Supervisors:

Einar HEIBERG PhD	Anders BJÖRKMAN MD PhD
Associate Professor	Adjunct Professor in Hand Surgery
Cardiac MR Group	Dept. of Translational Medicine
Lund University	Medical Faculty, Lund University
Director, Skåne University Hospital	Senior Consultant Dept of
3D printing Centre	Specialized Surgery - Hand Surgery
	Skåne University Hospital, Malmö

Examiner:

Karl ÅSTRÖM
Professor
Centre for Mathematical Sciences
Lund University

Lund University
Faculty of Engineering
Centre for Mathematical Sciences
FMAM05
Mathematical Sciences

June 15, 2020

LUND UNIVERSITY

Abstract

Faculty of Engineering
Centre for Mathematical Sciences

MSc Engineering Physics

Patient-Specific 3D Printed Guides for Corrective Osteotomies of Malunited Radius

by Carolin SKYBORN

The purpose of this master thesis was to expand an existing medical modelling software, Segment 3DPrint, and develop a tool for surgical planning for corrective osteotomy of the forearm. Fractures of the forearm are very common and in some patients the fractured bone unites abnormally, causing a deformation. This is called a malunion and can affect the functionality of the wrist. The patients experience this as impaired rotation of the forearm or impaired extension and flexion of the wrist in addition to pain. The surgical planning tool aims to create a patient-specific cutting guide to be used intraoperatively during corrective surgery where the deformed bone is corrected. During the operation the guide will be placed on the malunited bone and outline the location and angle for the cut as well as where to drill the holes for a fixation plate. The primary focus is on radius malunion but this project will serve as a basis for other parts of the human body in the future.

The process starts with 3D computed tomography (CT) images of the malunited radius and the contralateral, healthy, radius of the patient. The contralateral radius is mirrored in the software and used as a reference for the reconstruction of the malunited radius. The alignment of the malunited radius is performed by using intensity based image registration. After initial registration, the developed planning tool allows the user to adjust the alignment if necessary or otherwise desired. Both the proximal and distal ends of the radius are aligned to the healthy contralateral radius. A preferred location of the surgical cut is marked, followed by reconstruction of the deformed radius in compliance with proximal and distal alignment. When the desired anatomy of the reconstructed radius is achieved, the aligning information is translated back to the malunited radius, thus providing support for the design of the surgical cutting guide.

Keywords: Osteotomy, Radius malunion, 3D, 3D printing

Acknowledgements

I would like to give a special thank you to my supervisors Einar Heiberg and Anders Björkman. Without you this project would not have been possible.

Thank you Einar for all help and guidance throughout this project and for taking time even though you had none. Your knowledge amazes me and working with you has been very educational.

Thank you Anders for sharing patient cases and valuable input from the clinical aspect of this project, our meetings and discussions have been invaluable.

A big thank you to the Heart MR Group at Klinfys, Lund and the Medviso team for being available for questions and support at all times. The work environment during this project have been very enjoyable.

I would like to thank Philip Bernborg for your printing and CAD services, it has been a great help. Your help with the fixation plate made the very first cutting guide models possible.

Thank you Giuseppe Bianco at the Biology Department for great help with scanning our DVR plates.

Finally, I would like to thank my amazing family and friends for support and encouragement throughout my studies and this project. A special thank you to my wonderful fiancé Martin for always being there.

Contents

Abstract	iii
Acknowledgements	v
1 Introduction	1
2 Background	3
2.1 Anatomy	3
2.2 Symptomatic radius malunion	5
2.3 Benefits of cutting guides	5
3 Aim	7
4 Theory	9
4.1 Intensity based image registration	9
4.1.1 Rigid transformation	10
Two dimensions	11
Three dimensions	11
4.2 Monomodal image registration	12
4.2.1 Bilinear interpolation	12
4.2.2 Mean squared difference	15
4.2.3 Regular step gradient descent	15
4.3 Multimodal image registration	16
5 Methodology	17
5.1 Patient cases	17
5.1.1 Patient A	17
5.1.2 Patient B	17
5.1.3 Patient C	19
5.2 Two dimensional test case	19
5.2.1 Registration process	20
5.2.2 Reconstruction process	23
5.3 Three dimensional reconstruction	24
5.3.1 Aligning process	24
5.3.2 Plate placement	26
5.4 3D model of a surgical cutting guide	26
6 Results	27
6.1 Patient A	28
6.2 Patient B	29
6.3 Patient C	32

7 Discussion	39
7.1 Limitations	40
7.2 Future work	40
8 Conclusions	41
Bibliography	43
A Results patient A	45
B Results patient B	51
C Populärvetenskaplig sammanfattning	59

List of Figures

1.1	Anatomy of the right forearm, radius and ulna. Source: Atlas of Anatomy[1]	1
2.1	Articular surfaces of the radius and ulna of the right forearm. Source: Atlas of Anatomy[1]	3
2.2	Joint anatomy of the right forearm. Source: Atlas of Anatomy[1]	3
2.3	Movement of the radius, the red line marks the axis of supination/pronation. Source: Atlas of Anatomy[1]	4
2.4	Plates used in this project, only the NLP has points implemented in the software for the drill guides.	6
4.1	Illustration of the image registration process. If no initial transform exists, this input will be empty and will not affect the deformed image.	10
4.2	Illustration of the bilinear interpolation algorithm.	13
5.1	Patient A. Left radius healthy, right radius deformed.	18
5.2	Patient B. Left radius healthy, right radius deformed.	18
5.3	Patient C. Left radius deformed, right radius healthy. The figure shows the two bones from two different angles to better view the rotation deformity.	19
5.4	Appearance of schematic bones used for the 2D test case.	20
5.5	Area marked in red used for image registration of distal ends.	20
5.6	Distal image registration. The pink represents the deformed bone and the green represents the reference bone. White represents the area where the two bones overlap.	21
5.7	Area marked in red used for image registration of proximal ends.	21
5.8	Proximal image registration. The pink represents the deformed bone and the green represents the reference bone. White represents the area where the two bones overlap.	22
5.9	Reconstruction step for two dimensional test case. The red lines represent placement of the cut, the white part of the bottom image represents overlap meaning there is a collision of the two image parts.	23
5.10	Flow chart of the reconstruction process for three dimensions. Red is the deformed bone, green is the mirrored reference bone.	25
6.1	Patient A alignment (right radius malunion), dark grey is the mirrored reference bone, light grey is the deformed radius.	28
6.2	Patient A plate placement (right radius malunion).	29
6.3	Patient B alignment (right radius malunion), dark grey is the mirrored reference bone, light grey is the deformed radius.	30
6.4	Patient B, proximal alignment using a registration boundary below the radial tuberosity.	30
6.5	Patient B plate placement (right radius malunion).	31

6.6	Patient C alignment (left radius malunion), dark grey is the mirrored reference bone, light grey is the deformed radius.	32
6.7	Patient C reconstruction process (left radius malunion), dark grey is the mirrored reference bone, light grey is the deformed radius.	33
6.8	Patient C reconstruction process (left radius malunion), dark grey is the mirrored reference bone, light grey is the deformed radius.	34
6.9	Patient C plate placement (left radius malunion).	35
6.10	Patient C cutting guide (left radius malunion).	36
6.11	Patient C cutting guide placement on deformed left radius.	37
A.1	Patient A reconstruction process (right radius malunion), dark grey is the mirrored reference bone, light grey is the deformed radius.	45
A.2	Patient A reconstruction process (right radius malunion), dark grey is the mirrored reference bone, light grey is the deformed radius.	46
A.3	Patient A plate placement (right radius malunion).	47
A.4	Patient A cutting guide (right radius malunion).	48
A.5	Patient A cutting guide placement on deformed right radius.	49
A.6	Patient A plate placement using the DVR plate (right radius malunion). 50	
B.1	Patient B, proximal alignment with registration boundary below the radial tuberosity compared to boundary above the radial tuberosity.	52
B.2	Patient B reconstruction process (right radius malunion), dark grey is the mirrored reference bone, light grey is the deformed radius.	53
B.3	Patient B reconstruction process (right radius malunion), dark grey is the mirrored reference bone, light grey is the deformed radius.	54
B.4	Patient B plate placement (right radius malunion).	55
B.5	Patient B cutting guide (right radius malunion).	56
B.6	Patient B cutting guide placement on deformed right radius.	57
C.1	Högra underarmens anatomi, radius and ulna. Källa: Atlas of Anatomy Image Collection, Thieme Publishing Group.	59
C.2	Kap- och bormmall med passning för felställt radiusben.	60

Chapter 1

Introduction

The forearm contains two long bones, the radius and the ulna (cubitus bone), see Figure 1.1.



Figure 1.1: Anatomy of the right forearm, radius and ulna. Source: Atlas of Anatomy[1]

Fractures of the forearm where either the radius or the ulna or both are fractured are very common and most often affect the distal third of the forearm, i.e. the wrist. Forearm fractures usually heal well without greater deformation of the

injured bones, but in some patients there is a malunion, meaning the fragments of the fractured bone unites in an abnormal position. This often results in problems for the patients in terms of pain and limited mobility of the forearm or the wrist i.e. the joint is functionally impaired. A malunited fracture of the forearm is usually corrected surgically with an osteotomy. This means the deformed bone is surgically cut and realigned and subsequently fixated using a metal plate in order to stabilise the osteotomy and thus allow the bone to heal. This type of procedure is often performed freehand by the surgeon i.e. no aids except measurement instruments are used to show where the bone should be cut and what angle it should be cut in. To prepare the procedure standardised two dimensional X-ray images are used to plan the reconstruction. During the procedure the surgeon then decides the location and angle of the cut. For more complex cases it can be difficult during surgery to realise how the fractured bone needs to be cut in order to create the preferred alignment. For these cases a pre-designed and patient-specific cutting guide can be used. This guide shows the surgeon where to cut the bone and in what angle in order to achieve the preferred correction.

As of today these guides are designed and produced by specialised companies abroad. The process is expensive and thus it is seldom used within the Swedish health care system, except for the most complicated cases.

The aim of this master thesis was to create a methodology based on medical image analysis and mathematical optimisation in order to extract satisfactory angles for cutting and with these create a cutting guide. This cutting guide is to be designed in a three dimensional modelling environment using Segment 3DPrint software. After 3D modelling the guide will be printed using the software, sterilised and used during the procedure as a surgical guide.

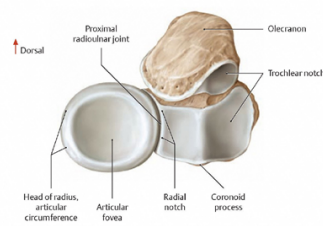
The idea is to use established methods within medical image analysis to perform image registration of the deformed bone on a healthy reference bone. This in order to align the deformed bone to the reference bone. Preferably, this is performed by using a mirrored version of the patient's healthy side as a reference and the deformed side is then aligned to this reference. By aligning the deformed bone to a reference and using this alignment to create a surgical cutting guide on site opens up for more accessibility. Easier access to these cutting guides and to a lower cost will in turn open up for further improvements of the methodology that is currently in use for corrective osteotomies. Furthermore the improved accessibility of 3D printed cutting guides can improve the quality of care given to patients as well as decrease the cost and improve the outcome of surgical procedures[2, 3].

Chapter 2

Background

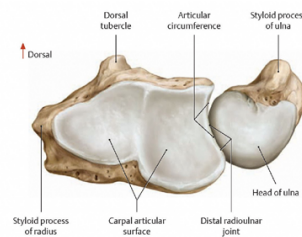
2.1 Anatomy

The radius and the ulna are joined in the elbow (the proximal radio-ulnar joint, PRUJ), see Figure 2.1a as well as in the wrist (the distal radio-ulnar joint, DRUJ)[4], see Figure 2.1b. In the elbow joint the two forearm bones joins together with the humerus, see Figure 2.2a and in the wrist they join together with proximal carpal row i.e. the scaphoid, lunate and triquetrum[5], see Figure 2.2b.



The proximal articular surfaces of the radius and ulna of the right forearm. Proximal view

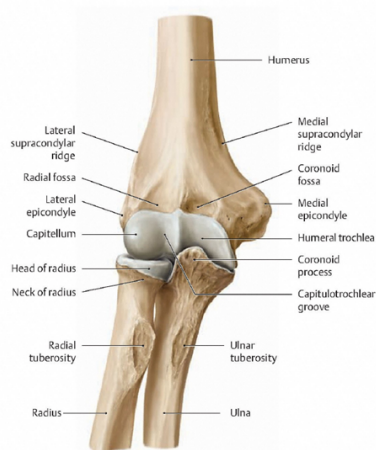
(a) Proximal view.



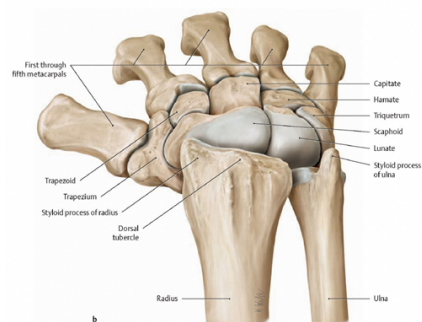
The distal articular surfaces of the radius and ulna of the right forearm. Distal view

(b) Distal view.

Figure 2.1: Articular surfaces of the radius and ulna of the right forearm. Source: Atlas of Anatomy[1]



(a) Elbow joint, anterior view.



(b) Wrist joint, posterior view.

Figure 2.2: Joint anatomy of the right forearm. Source: Atlas of Anatomy[1]

In the elbow joint, the proximal ulna and the distal humerus joins together in a synovial hinge joint, whereas the head of radius articulates against the humerus and ulna and is wrapped in ligaments allowing the radius to rotate through pronation and supination of the forearm[4], see Figure 2.3. From a functional point of view, the elbow can flex and extend. Forearm rotation is done both in the elbow and in the distal radio-ulnar joint in the wrist.

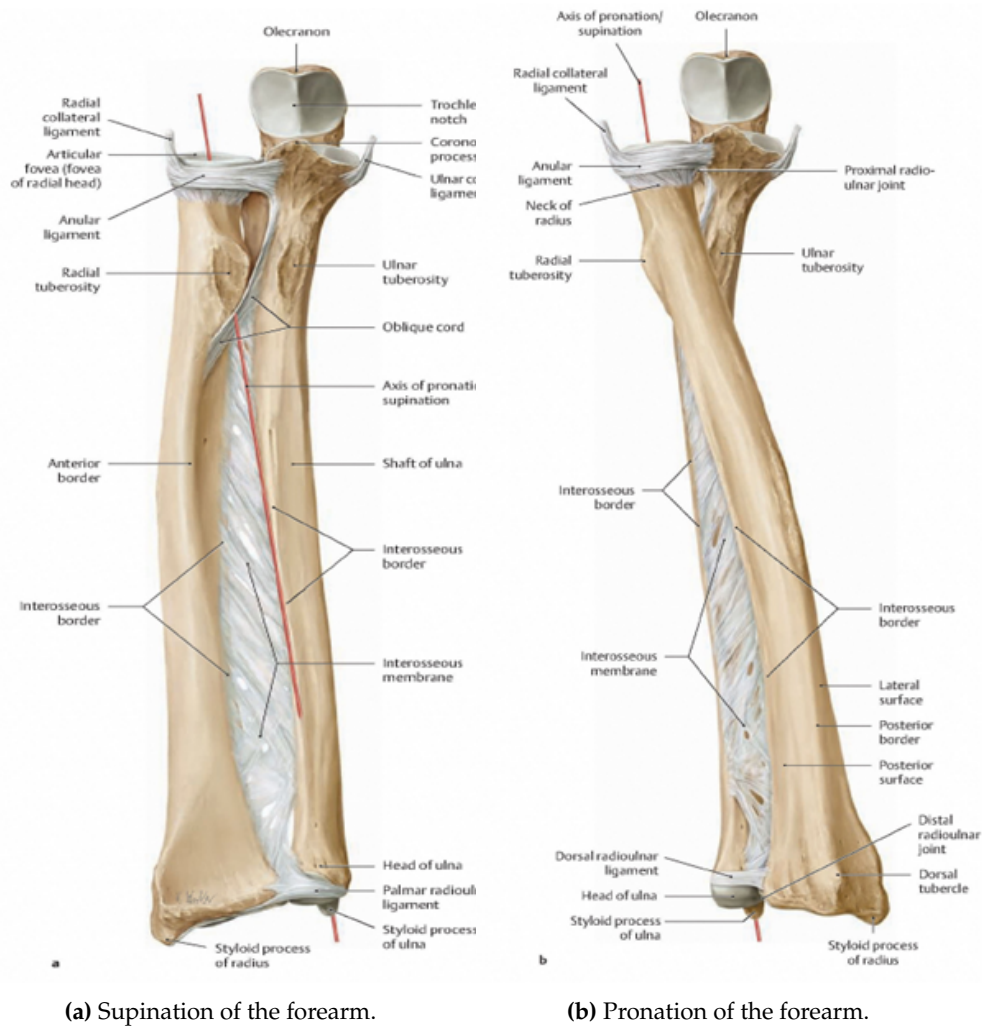


Figure 2.3: Movement of the radius, the red line marks the axis of supination/pronation. Source: Atlas of Anatomy[1]

In the wrist the distal radius and the carpal bones joins in an ellipsoid joint (the radio-carpal joint) which allows wrist extension and flexion of the hand as well as radial and ulnar deviation[6–8]. The ulna is not part of the wrist joint but it articulates with the distal radius in the DRUJ and helps provide stability in the forearm through pronation and supination[5]. The longitudinal stability in the forearm is provided mainly by the radial head, see Figure 2.2a and the interosseous membrane[7] attaching the radial and ulnar shaft to each other, see Figure 2.3.

Some muscles that have their attachment on the radius and are involved in the function of the forearm are the following: The *brachioradialis* which starts at the lateral epicondyle of the humerus, see Figure 2.2a, and attaches on the distal radius, performing flexion of the elbow[9] and also providing some supination of the forearm[10]. The *pronator teres* starts at both the medial epicondyle of the humerus and the coronoid process, see Figure 2.2a, on the ulna and attaches on the middle of the radius, performing pronation of the forearm as well as providing some flexion of the elbow[9]. The *pronator quadratus* is also involved in pronation of the forearms. This muscle starts at the distal ulna and attaches at the distal radius[9]. The *biceps brachii* and the *supinator*, together with the brachioradialis as mentioned, are all involved in supination of the forearm[10]. Biceps brachii starts at the scapula and attaches on the radial tuberosity, see Figure 2.2a. The supinator starts at both the lateral epicondyle of the humerus and the proximal ulna and attaches on the middle, lateral side, of the radius providing both supination (humerus attachment) and forearm stability (ulna attachment)[10].

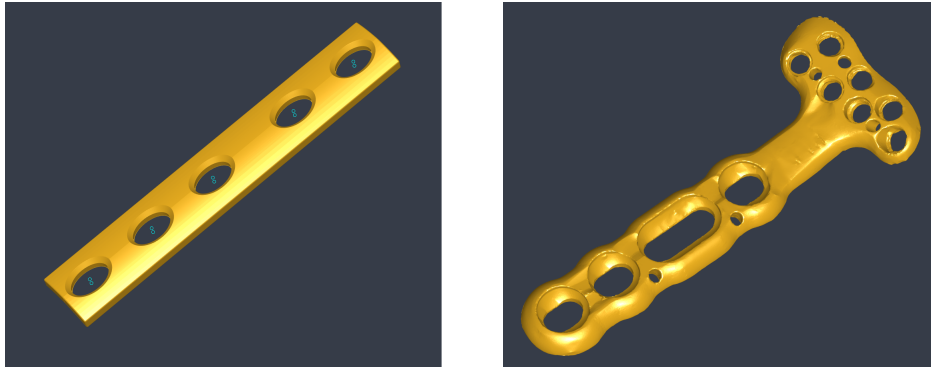
2.2 Symptomatic radius malunion

When a patient experiences a fracture of the distal radius followed by a malunion some common symptoms are: pain and discomfort, decreased grip strength, decreased range of motion in both extension and flexion as well as radial/ulnar abduction[11]. If left untreated there is an increased risk of damage to the articular surface in the wrist joint and subsequently the development of arthritis[12]. For corrective osteotomies of a malunited radius it is important that the alignment in both the proximal and distal end is restored in order to preserve mobility of the forearm[7].

2.3 Benefits of cutting guides

The reported benefits of using a cutting guide are many, e.g. decreased time for the surgical procedure which in itself is cost effective[2, 3] but it may also reduce the risk of surgical site infection (SSI). SSI is caused by bacteria that infect the surgical wound, e.g. through contaminated surgical equipment or through bacteria existing on the skin of the patient[13]. The longer the operative time, the higher is the risk for SSI[14]. Furthermore the usage of a cutting guide increases the precision of the procedure[2] which argues for better and faster fracture healing as well as increased overall functional performance for the patient. Several randomised controlled trials (RCT) where 3D printed anatomical models are used for pre surgical planning, indicate said benefits although not statistically significant[2]. These models include both anatomical guides designed to aid the surgeon during the operation as well as 3D printed anatomical implants. The usage of anatomical guides can decrease operating time and increase precision[2]. The usage of 3D printed implants indicate increased cost effectiveness due to the 3D printing being relatively cheap in comparison to prior production cost of surgical implants[15].

There are several fixation plates that can be used when stabilising the osteotomy. For distal radius malunions an anatomically shaped plate is often preferred e.g. a DVR[®] plate which stands for *Distal Volar Radius*, see Figure 2.4b. For cuts placed more proximally a straight non locking plate (NLP) may be of better use, see Figure 2.4a. The NLP presented in Figure 2.4 is used for all proposed reconstructions performed in this project as well as the making of the cutting guides. An alternative plate placement is presented for one patient using the DVR plate, see Appendix A.



(a) Non locking plate (NLP).

(b) DVR plate.

Figure 2.4: Plates used in this project, only the NLP has points implemented in the software for the drill guides.

Chapter 3

Aim

Skåne University Hospital is currently lacking the competence and tools needed to create their own 3D printed cutting guides. This master thesis aims to take advantage of the 3D printing possibilities that exists within the hospital and implement a tool that will make it possible to create surgical cutting guides on site.

In order to create a planning environment that provides a good overview of a patient case the thesis aim to implement a graphical user interface with the following functions:

- The ability to align objects together with manual rotation and translation.
- The ability to cut an object using a rotatable plane in 3D space. To implement a mathematical optimisation regarding placement of said cut.
- The ability to use registration transformations together with manual transformations to extract reconstruction information.
- Functionality to perform proof-of-concept creation of cutting guides.

Chapter 4

Theory

Usually when it comes to medical images an intensity based image registration method is beneficial. Mostly due to the fact that this method does not require any presumptions to be made about the images. Furthermore the occurrence of features in the images is not always significant[16]. This type of registration technique works well for large sets of images and it is automated which can be valuable for saving manual labour[17]. When it comes to medical images the image pair is either taken with the same modality (*monomodal*) or they are taken with two different modalities (*multimodal*). The intensity based image registration technique is self-evident for registration of images from the same modality and the deformation between an image pair can be considered small.

4.1 Intensity based image registration

Intensity based image registration uses a *metric*, an *optimiser* and a *transformation type* to iteratively align one image to another. The technique maps the pixels in the image pairs using each image's relative intensity pattern[17]. In this thesis a rigid transform is used for the registration process. The rationale for this is that the parts to be registered, the malunited and the mirrored contralateral part, are geometrically similar. For this master thesis the images regarded for the registration process will be referred to as follows:

- **Reference image/reference bone**, image volume consisting of a healthy radius. This image has the desired outcome of the reconstruction.
- **Deformed image/deformed bone**, image volume consisting of a malunited radius. This image is to be transformed into alignment with the reference image.

Depending on whether the images are monomodal or multimodal the optimiser and metric differs in the registration process. The registration process is similar however and starts with specifying what transform type that is to be used. One can also use an initial transformation matrix e.g. if several images are to be registered to the same reference image and they all have similar spatial displacement. If there exists an initial transformation matrix then this matrix is applied to the deformed image by *bilinear interpolation*. When the deformed image has been resampled it is compared to the reference image using the specified similarity metric. If no initial transformation matrix exists the deformed image is compared to the reference image without resampling. A metric value for the similarity between the deformed image and the reference image is computed. The last step is the optimiser which checks

whether this metric value meets a stop condition or not. If the metric value does not agree with the stop condition the optimiser creates a new transformation matrix based on the previous one, if such a matrix exists. The process then starts over with this new transformation matrix, see Figure 4.1 for overview. The stop condition is met either when the metric value is below a certain tolerance or when the process reaches the maximum number of iterations, both of which values can be changed manually.

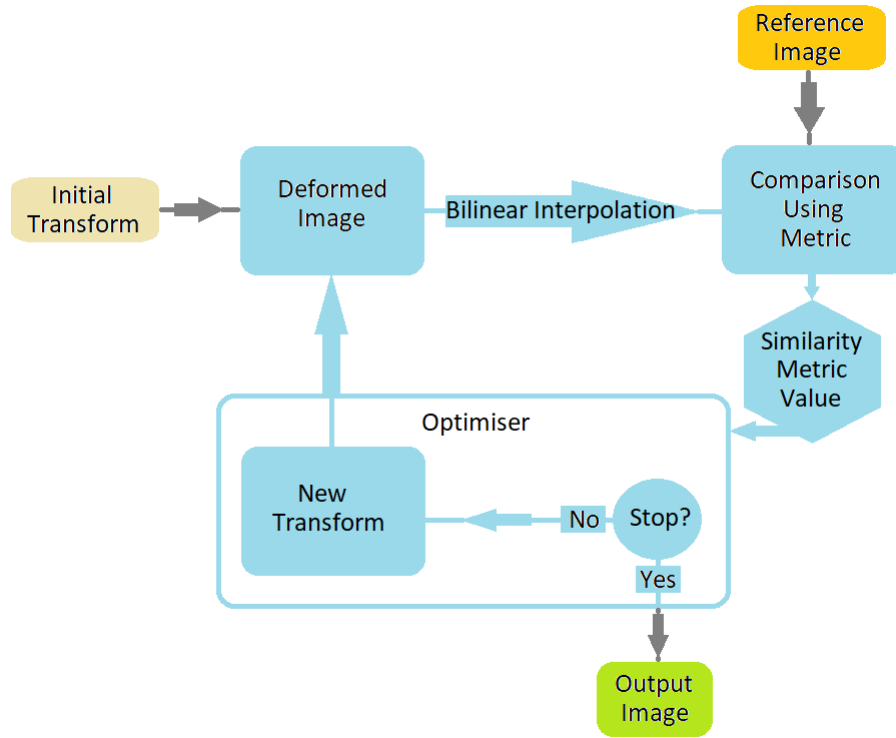


Figure 4.1: Illustration of the image registration process. If no initial transform exists, this input will be empty and will not affect the deformed image.

4.1.1 Rigid transformation

Rigid transformation involves rotation and translation. This gives the transformation parameters for two and three dimensions as

$$\begin{aligned}\Theta_{2D} &= [\alpha \ t_x \ t_y] , \\ \Theta_{3D} &= [\alpha_x \ \alpha_y \ \alpha_z \ t_x \ t_y \ t_z] ,\end{aligned}\tag{4.1}$$

where α is the angle of rotation and t_x, t_y, t_z represents the translation along x, y and z axis respectively. A rigid transform with rotation and translation in two dimensions is represented as

$$\mathbf{T} = \begin{bmatrix} x \cos(\alpha) - y \sin(\alpha) + t_x \\ x \sin(\alpha) + y \cos(\alpha) + t_y \end{bmatrix} .\tag{4.2}$$

Two dimensions

For two dimensions the matrix representation of the geometric transform contains rotation about the z-axis as well as translation in x and y direction. The image registration is rigid, thus there is no scaling present. Rotation is represented as

$$R = \begin{bmatrix} \cos(\alpha) & \sin(\alpha) & 0 \\ -\sin(\alpha) & \cos(\alpha) & 0 \\ 0 & 0 & 1 \end{bmatrix}, \quad (4.3)$$

where α is the angle of rotation about the origin, which in image processing corresponds to the upper left corner. For this reason the geometric matrices will be transposed compared to the transformation parameters presented in (4.2). Translation is represented as

$$t = \begin{bmatrix} 1 & 0 & 0 \\ 0 & 1 & 0 \\ t_x & t_y & 1 \end{bmatrix}, \quad (4.4)$$

where t_x is the translation along the x-axis and t_y is the translation along the y-axis[18]. Again, the translation matrix is transposed compared to the transformation parameters in (4.2) due to the fact that the image origin is the upper left corner of an image.

Three dimensions

The matrix representation for the geometric transform in three dimensions look as follows. For translation there is only the added translation along the z-axis, t_z

$$t = \begin{bmatrix} 1 & 0 & 0 & 0 \\ 0 & 1 & 0 & 0 \\ 0 & 0 & 1 & 0 \\ t_x & t_y & t_z & 1 \end{bmatrix} \quad (4.5)$$

and the rotation is represented about each axis separately as

$$R_x = \begin{bmatrix} 1 & 0 & 0 & 0 \\ 0 & \cos(\alpha_x) & \sin(\alpha_x) & 0 \\ 0 & -\sin(\alpha_x) & \cos(\alpha_x) & 0 \\ 0 & 0 & 0 & 1 \end{bmatrix}, \quad (4.6)$$

$$R_y = \begin{bmatrix} \cos(\alpha_y) & 0 & -\sin(\alpha_y) & 0 \\ 0 & 1 & 0 & 0 \\ \sin(\alpha_y) & 0 & \cos(\alpha_y) & 0 \\ 0 & 0 & 0 & 1 \end{bmatrix}, \quad (4.7)$$

$$R_z = \begin{bmatrix} \cos(\alpha_z) & \sin(\alpha_z) & 0 & 0 \\ -\sin(\alpha_z) & \cos(\alpha_z) & 0 & 0 \\ 0 & 0 & 1 & 0 \\ 0 & 0 & 0 & 1 \end{bmatrix}, \quad (4.8)$$

where α_x , α_y and α_z is rotation about each axis. Total rotation represents rotation about the x-axis first, then rotation about y-axis and then rotation about z-axis. This is computed by right-side multiplication of the rotation matrices

$$R_{tot} = R_z R_y R_x = \begin{bmatrix} c(\alpha_z)c(\alpha_y) & s(\alpha_z)c(\alpha_x) + c(\alpha_z)s(\alpha_y)s(\alpha_x) & s(\alpha_z)s(\alpha_x) - c(\alpha_z)s(\alpha_y)c(\alpha_x) & 0 \\ s(\alpha_z)c(\alpha_y) & c(\alpha_z)c(\alpha_x) + s(\alpha_z)s(\alpha_y)s(\alpha_x) & s(\alpha_z)s(\alpha_y)c(\alpha_x) - c(\alpha_z)s(\alpha_x) & 0 \\ s(\alpha_y) & -c(\alpha_y)s(\alpha_x) & c(\alpha_y)c(\alpha_x) & 0 \\ 0 & 0 & 0 & 1 \end{bmatrix}, \quad (4.9)$$

where $c(\alpha)$ and $s(\alpha)$ represents $\cos(\alpha)$ and $\sin(\alpha)$ respectively.

4.2 Monomodal image registration

For images taken with the same scanner (modality) and with the same exposure settings the problem at hand is usually a spatial displacement between the image pairs. This displacement can originate from the images being acquired at different times. The intensity patterns will be similar since the relative intensity for a tissue type, e.g. bone tissue, will be the same for both images. The image pairs used for this master thesis are acquired using the same modality (CT) and settings. The images used for the registration are not the CT images per se but an approximated truncation of the distance transform of the segmentation of the bones. This makes the monomodal registration approach suitable. For monomodal image registration the *mean squared difference* method is used for the similarity measurement and the optimiser is *regular step gradient descent*[17].

4.2.1 Bilinear interpolation

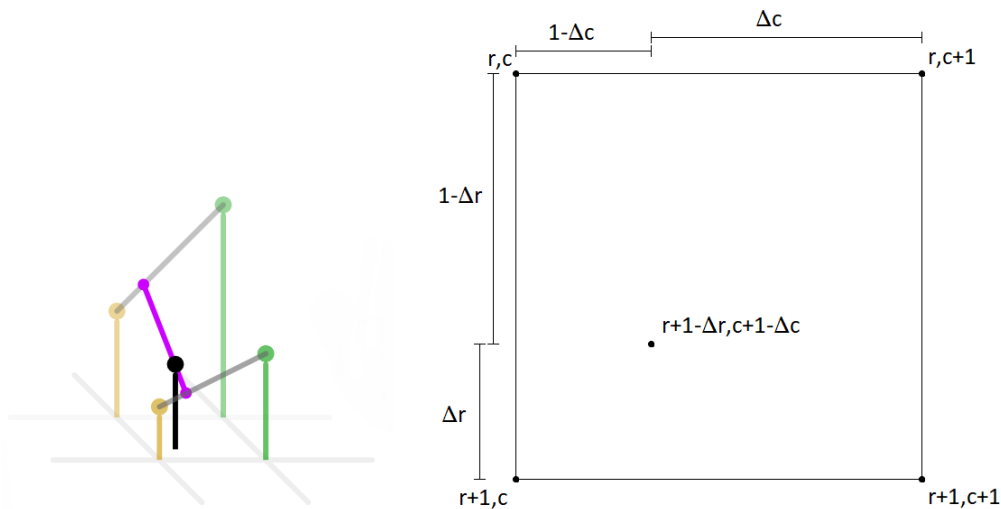
This interpolation method takes the weighted mean of adjacent pixel values to compute the new pixel value[19]. For example, take the input image

$$\begin{array}{ccc} 1 & 2 & 3 \\ 4 & 5 & 6 \\ 7 & 8 & 9 \end{array}$$

If this image is to be translated 0.66 pixels in positive horizontal direction and 0.33 pixels in positive vertical direction the procedure works as follows. First, the image is zero padded, then the image is translated as illustrated below. The bold numbers represent the original input image and the plain numbers represent the translated input image.

$$\begin{array}{ccccc}
 0 & 0 & 0 & 0 & 0 \\
 & \mathbf{1} & \mathbf{2} & \mathbf{3} & \mathbf{0} \\
 0 & 1 & 2 & 3 & 0 \\
 & \mathbf{4} & \mathbf{5} & \mathbf{6} & \mathbf{0} \\
 0 & 4 & 5 & 6 & 0 \\
 & \mathbf{7} & \mathbf{8} & \mathbf{9} & \mathbf{0} \\
 0 & 7 & 8 & 9 & 0 \\
 & \mathbf{0} & \mathbf{0} & \mathbf{0} & \mathbf{0} \\
 0 & 0 & 0 & 0 & 0
 \end{array} \tag{4.10}$$

The output image is computed by replacing the bold pixel values with the weighted mean of the surrounding four plain pixel values. The weight is the distance from each surrounding pixels. The interpolation is performed in one direction first, then the other. The first two rows and columns from (4.10) are displayed in Figure 4.2 together with an illustration of the bilinear interpolation. The same result is achieved regardless of what direction is interpolated first, the formula in (4.11) interpolates horizontally first and then vertically but one may just as well start vertically and then proceed with horizontal interpolation.



(a) Bilinear interpolation. Source: (Modified) Wikimedia [20]

(b) The pixel inside the square represents the original input image, the pixels at the corners represents the zero padded translated input image.

Figure 4.2: Illustration of the bilinear interpolation algorithm.

The output pixel values are calculated using the following formula:

$$\begin{aligned}
I_{r,c+1-\Delta c}^{out} &= \frac{(c+1) - (c+1 - \Delta c)}{(c+1) - c} \cdot I_{r,c}^{trans} + \frac{(c+1 - \Delta c) - c}{(c+1) - c} \cdot I_{r,c+1}^{trans} \\
&= \Delta c \cdot I_{r,c}^{trans} + (1 - \Delta c) \cdot I_{r,c+1}^{trans} \\
I_{r+1,c+1-\Delta c}^{out} &= \frac{(c+1) - (c+1 - \Delta c)}{(c+1) - c} \cdot I_{r+1,c}^{trans} + \frac{(c+1) - (c+1 - \Delta c)}{(c+1) - c} \cdot I_{r+1,c+1}^{trans} \\
&= \Delta c \cdot I_{r+1,c}^{trans} + (1 - \Delta c) \cdot I_{r+1,c+1}^{trans} \\
I_{r+1-\Delta r,c+1-\Delta c}^{out} &= \frac{(r+1) - (r+1 - \Delta r)}{(r+1) - r} \cdot I_{r,c+1-\Delta c}^{out} + \frac{(r+1 - \Delta r) - r}{(r+1) - r} \cdot I_{r+1,c+1-\Delta c}^{out} \\
&= \Delta r \cdot I_{r,c+1-\Delta c}^{out} + (1 - \Delta r) \cdot I_{r+1,c+1-\Delta c}^{out} \\
&= \Delta r (\Delta c \cdot I_{r,c}^{trans} + (1 - \Delta c) \cdot I_{r,c+1}^{trans}) \\
&\quad + (1 - \Delta r) (\Delta c \cdot I_{r+1,c}^{trans} + (1 - \Delta c) \cdot I_{r+1,c+1}^{trans})
\end{aligned} \tag{4.11}$$

Here, I^{out} is the interpolated output image and I^{trans} is the translated input image. Δr and Δc represents the distances from the translated image row and column to the original image row and column as shown in Figure 4.2. With $\Delta r = 0.33$ (vertical translation) and $\Delta c = 0.66$ (horizontal translation) the output pixel value for $I_{r,c}^{out}$ will be:

$$\begin{aligned}
I_{r,c}^{out} &= 0.33 [0.66 \cdot I_{r,c}^{trans} + (1 - 0.66) \cdot I_{r,c+1}^{trans}] + (1 - 0.33) [0.66 \cdot I_{r+1,c}^{trans} + (1 - 0.66) \cdot I_{r+1,c+1}^{trans}] \\
&= 0.2178 \cdot I_{r,c}^{trans} + 0.1122 \cdot I_{r,c+1}^{trans} + 0.4422 \cdot I_{r+1,c}^{trans} + 0.2278 \cdot I_{r+1,c+1}^{trans}
\end{aligned} \tag{4.12}$$

This formula gives the output pixel value for $I_{1,1}^{out} = 0.2178$ and the resulting output image is:

0.2178	0.5478	0.8778	0.3366
1.3134	2.6500	3.6500	1.3566
3.2934	5.6500	6.6500	2.3766
3.0954	5.1322	5.8022	2.0502

Notice that the output image have one extra row and column. This is due to the translation and can be altered if desired. If the output image is preferred to have the same size as the original input image, $[3 \times 3]$, the translation is rounded to the closest integer. In this case the output image will instead be

0.5478	0.8778	0.3366
2.6500	3.6500	1.3566
5.6500	6.6500	2.3766

where the first column and last row has been removed. This is due to the vertical translation being rounded to one: $\Delta c = 0.66 \approx 1$, which leads to the first column being removed and the horizontal translation being rounded to zero: $\Delta r = 0.33 \approx 0$, which leads to the last row being removed.

4.2.2 Mean squared difference

The mean squared difference algorithm (MSD) takes the squared difference in corresponding pixels in the two images. The mean of these differences is then computed and the result is a scalar value which represents the metric value given to the optimiser. The formula is

$$MSD(\Theta_t) = \frac{1}{N} \sum_{i \in \Omega_{r,d}} [I_r(i) - I_d(\mathbf{T}(i; \Theta_t))]^2, \quad (4.13)$$

where $I_r(i)$ is the intensity of the i^{th} pixel in the reference image and $I_d(\mathbf{T}(i; \Theta_t))$ is the intensity of the *transformed* i^{th} pixel in the deformed image with respect to the transformation parameters Θ_t . $\Omega_{r,d}$ is the region where the two images overlap, the *intersection* of I_r and I_d , and N is the number of pixels in said overlap. Θ_t represents the transformation parameters for the current process iteration. When using MSD it is important that the image intensities are similar. This is rarely the case for multimodal registration and the measure is therefore used mostly for monomodal registration[21]. Still, with monomodal registration one needs to be mindful of the possibility of different settings for the images if these have been acquired either at different times or by different sequences. Since the images in this thesis are acquired simultaneously the MSD measure is a good choice for the metric.

4.2.3 Regular step gradient descent

The regular step gradient descent algorithm is the optimiser for the registration process[22, 23]. It aims to minimise the *sum* of squared differences which is the objective function of the registration process, referred to as the *error function*,

$$E(\Theta_t) = \sum_{i \in \Omega_{r,d}} [I_r(i) - I_d(\mathbf{T}(i; \Theta_t))]^2. \quad (4.14)$$

Note that the formula is identical to the MSD in (4.13) apart from not being divided by N . By minimising the error function the mean squared difference will of course also be minimised. The algorithm takes downhill steps in the negative gradient direction in order to minimise the error. The gradient is calculated numerically with respect to the transformation parameters Θ_t and the new parameters are computed as

$$\Theta_{t+1} = \Theta_t - a_t \nabla E(\Theta_t), \quad (4.15)$$

where a_t is the step size. The gradient of the error function can be computed using the chain rule on (4.14)

$$\frac{\partial E}{\partial \Theta} = \sum_{i \in \Omega_{r,d}} -2 [I_r(i) - I_d(\mathbf{T}(i; \Theta_t))] \frac{\partial I_d}{\partial \mathbf{T}} \frac{\partial \mathbf{T}}{\partial \Theta}, \quad (4.16)$$

where the first term in the sum, $[I_r(i) - I_d(\mathbf{T}(i; \Theta_t))]$, represent the error in the i^{th} pixel location. The second term, $\frac{\partial I_d}{\partial \mathbf{T}}$, represent the deformed image intensity gradient and the third term, $\frac{\partial \mathbf{T}}{\partial \Theta}$, represent the transformation gradient. When it comes to rigid rotation and translation the transformation parameters are $\Theta = (\alpha, t_x, t_y)$ (in two dimensions) with transformation gradient

$$\frac{\partial \mathbf{T}}{\partial \Theta} = \begin{bmatrix} -x \sin(\alpha) - y \cos(\alpha) & 1 & 0 \\ x \cos(\alpha) - y \sin(\alpha) & 0 & 1 \end{bmatrix} \quad (4.17)$$

derived from (4.2). The image intensity gradient is expressed in x and y components

$$\frac{\partial I_d}{\partial \mathbf{T}} = \begin{bmatrix} \frac{\partial I_d(\mathbf{T}(i; \Theta))}{\partial x} \\ \frac{\partial I_d(\mathbf{T}(i; \Theta))}{\partial y} \end{bmatrix} \quad (4.18)$$

and can be computed with a finite difference approximation which gives

$$\begin{aligned} \frac{\partial I_d(\mathbf{T}(i; \Theta))}{\partial x} &\approx \frac{I_d(x + \Delta x, y) - I_d(x, y)}{\Delta x} \\ \frac{\partial I_d(\mathbf{T}(i; \Theta))}{\partial y} &\approx \frac{I_d(x, y + \Delta y) - I_d(x, y)}{\Delta y} \end{aligned} \quad (4.19)$$

for two dimensions. This is computed for all pixels in the deformed image, a step is then taken in the negative gradient direction and the error is re-evaluated. If the gradient changes direction between iterations it is implied that a minimum of the objective function has been passed. The step size is reduced by multiplication with the relaxation factor which has default value 0.5[23]. Initial step size as well as the value of the relaxation factor can be adjusted. When the step size and/or the magnitude value of the gradient reaches a minimum value the iteration will stop, indicating that the optimisation has converged. This gradient descent algorithm has a linear convergence rate[22] and can be slow if the step size is chosen poorly, e.g. very small when image pairs are greatly misaligned. Furthermore this method may converge to a local minimum which is something to keep in mind.

4.3 Multimodal image registration

When images from different modalities are to be evaluated the multimodal approach is taken. This is also applicable for images from different scanners. The intensity patterns may differ between the image pairs either due to them being taken from two different modalities such as a CT and an MR image or when two different CT cameras are used with perhaps different brightness settings. The similarity metric used for multimodal image registration could for example be *mutual information*. Since the images comes from different modalities the correlation between corresponding pixel intensities are rarely linear which makes a similarity metric as the mean square difference of the pixel intensities a poor choice. Instead the mutual information is used, measuring the degree of dependence the image pairs have to each other. This can be done either by comparing the histogram of the joint image intensities[24], or by using the joint probability densities to get a measure of the entropies of the images and from these compute the mutual information[25, 26].

Chapter 5

Methodology

This chapter outlines the developed methodology of the performed tests.

5.1 Patient cases

The software from this master thesis have been validated using three patient cases, provided by Dr. Anders Björkman Department of Hand Surgery, Skåne University Hospital, Malmö. The purpose of the patient cases was to exemplify the technique used in the developed software. The patient cases are presented below.

5.1.1 Patient A

Patient A had a malunion on the right radius approximately 1/3 of the bone length from the distal joint surface, see Figure 5.1. The resulting deformation is a dorsal angulation meaning that the distal part of the radius deviates dorsally (posteriorly), as shown in Figure 6.1a. The original CT image have the size $[512 \times 512 \times 621]$ pixels with a resolution of $[0.39 \times 0.39 \times 0.60]$, giving a resolution ratio > 1.5 (largest pixel resolution divided by smallest pixel resolution). The image was resampled giving the size $[512 \times 512 \times 954]$ pixels with an isotropic resolution of $[0.39 \times 0.39 \times 0.39]$.

5.1.2 Patient B

Patient B had a malunion of the right radius following a fracture in the middle part of the radius, see Figure 5.2. The radial tuberosity appears damaged although it may be a natural anatomically deviation from the contralateral healthy radius. The resulting deformation is a radial inclination as well as a smaller longitudinal rotation, as shown in Figure 6.3a. The CT image have the size $[205 \times 506 \times 648]$ pixels with a resolution of $[0.63 \times 0.63 \times 0.45]$, giving a resolution ratio < 1.5 . The image was not resampled.

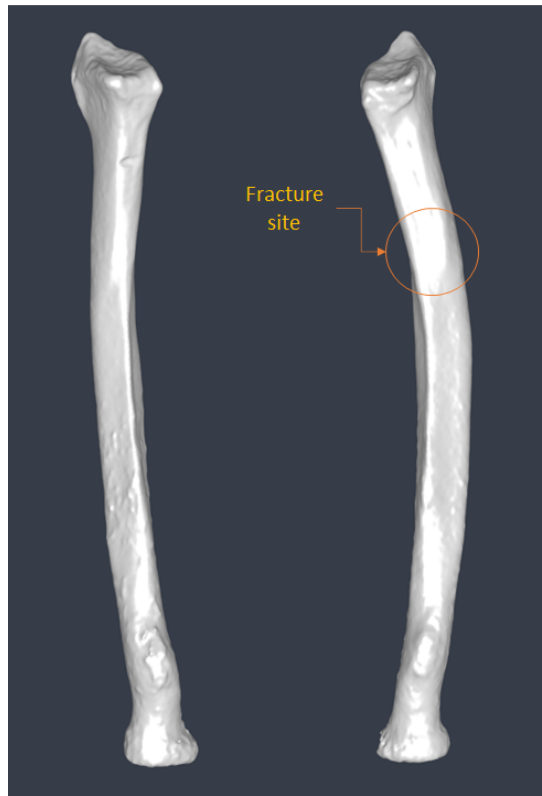


Figure 5.1: Patient A. Left radius healthy, right radius deformed.

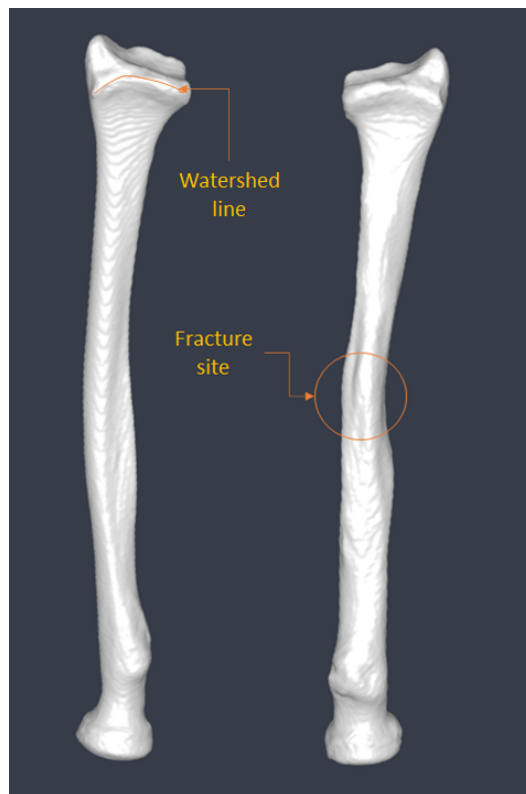


Figure 5.2: Patient B. Left radius healthy, right radius deformed.

5.1.3 Patient C

Patient C had a malunion of radius on the left hand side, see Figure 5.3. The resulting deformation is a slight dorsal angulation where the radius' distal end deviates posteriorly as well as a large longitudinal rotation of approximately 90 degrees, as shown in Figure 6.6a. The CT image have the size $[325 \times 718 \times 899]$ pixels with an isotropic resolution of $[0.40 \times 0.40 \times 0.40]$. The image was not resampled.

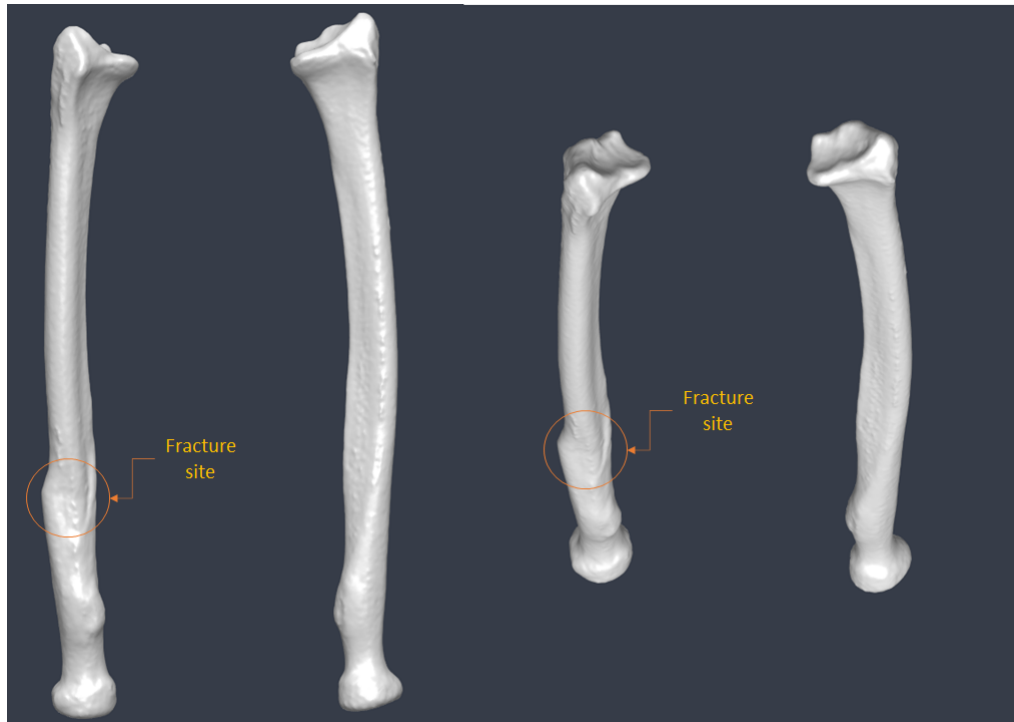


Figure 5.3: Patient C. Left radius deformed, right radius healthy. The figure shows the two bones from two different angles to better view the rotation deformity.

5.2 Two dimensional test case

To begin the project, a simplified two dimensional test case with a deformed bone was implemented. This test case as well as the main software for three dimensional models was implemented in Matlab[®] version 2019a, by MathWorks[®] Massachusetts, USA. The central idea with the test case was to try the image registration script on both translation and rotation differences between the reference bone and the deformed/fractured bone. A binary image indicating a healthy bone was created and used as a reference for the registration. This reference bone was then modified by cutting the image at the proximal end, below its articular surface, and rotating the proximal end, simulating a malunion of the bone. The appearance of both reference and deformed bone is displayed in Figure 5.4.

The rotation of the proximal end of the deformed bone was done using the Matlab function `imwarp`. This function applies a geometric transformation to the image via inverse mapping, meaning that the coordinates in the output image is mapped to its corresponding coordinates in the input image according to the geometric transform. The aforementioned coordinate mapping is then used to interpolate the pixel

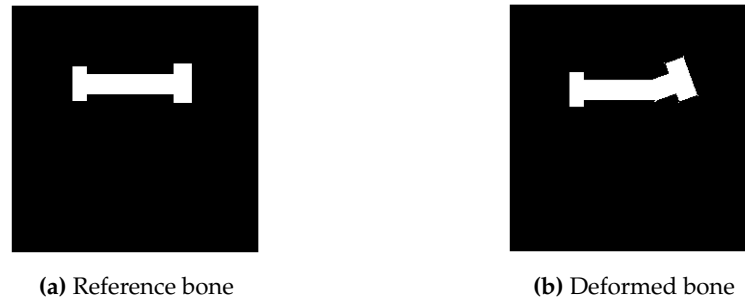


Figure 5.4: Appearance of schematic bones used for the 2D test case.

values, using bilinear interpolation, in the input image in order to get the output image pixel values[18]. This interpolation will leave the rotated output image as a non binary image with some pixel values slightly above or below the input image's pixel values.

5.2.1 Registration process

When both the reference bone and deformed bone has been created the next step is to perform the image registration. For good alignment at both ends of the deformed bone the registration needs to be executed for parts of the images, since they now differ from each other due to the deformation.

The idea explored in this thesis is to perform two separate image registrations, one distally as well as one proximally. Furthermore, the time consumed for the registrations is likely to improve for smaller image sizes, since computer tomography images of the forearm tends to be large depending on its resolution (the cases used in this thesis are of sizes $[512 \times 512 \times 954]$, $[205 \times 506 \times 648]$, $[325 \times 718 \times 899]$ pixels respectively). An initial registration is done on either ends of the bones, e.g. the distal ends, by cutting the bone at a preferred location and then cropping the image at the bounding box of the bone part as shown in Figure 5.5. The reference cut is matched to the size of the deformed cut in order to have the same sized images.

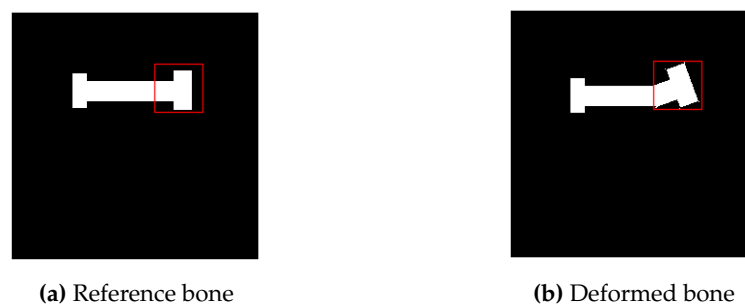


Figure 5.5: Area marked in red used for image registration of distal ends.

The image registration is performed on the areas marked by red in Figure 5.5. To get the geometric transformation matrix from the image registration the Matlab function `imregtform` is used, which gives the geometric transform as output. This function finds the best alignment of the deformed image to the reference image using

the optimisation algorithm explained in Chapter 4. The geometric transform is then applied to the deformed image using the `imwarp` function. The two images displayed together after the first registration is shown in Figure 5.6. If one wish to evaluate the success of the registration the dice score can be computed. It is a calculation of the overlapping pixels, marked as white in Figure 5.6, for the two images divided by total pixel count for the two images. This can be calculated for parts of the image or the full image. The formula for calculating the dice score is the following

$$DSC = \frac{2 \cdot [\sum_i I_r(i) \cap I_d(i)]}{\sum_i I_r + \sum_i I_d}, \quad (5.1)$$

where $I_r(i)$ and $I_d(i)$ represents pixel i in the images. This will give a score between 0 – 1 where 0 represents no overlap and 1 represents full overlap and perfect alignment.

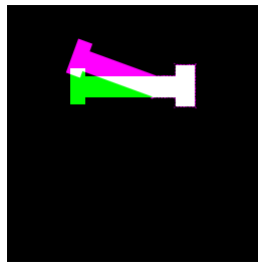


Figure 5.6: Distal image registration. The pink represents the deformed bone and the green represents the reference bone. White represents the area where the two bones overlap.

When the first image registration is performed and the distal parts of both bones are aligned the next step is to perform image registration on the proximal parts. A similar approach as the distal registration is taken and the proximal ends are cropped and handed to `imregtform` to get the geometric transformation matrix, see Figure 5.7.

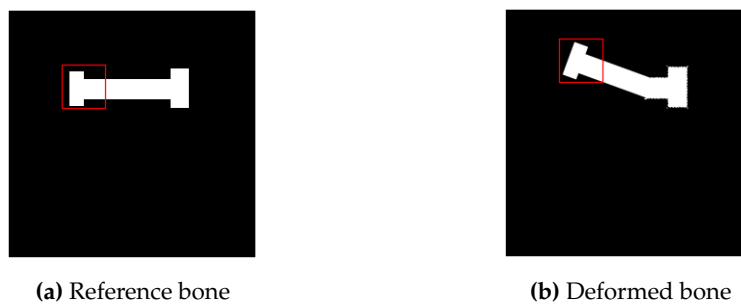


Figure 5.7: Area marked in red used for image registration of proximal ends.

The geometric transform is now calculated with the distal registration applied, meaning that this geometric transform can be interpreted as an internal deformation transform for the deformed bone, in order to align with the reference bone's distal and proximal ends. The two images displayed together after the second registration is shown in Figure 5.8.

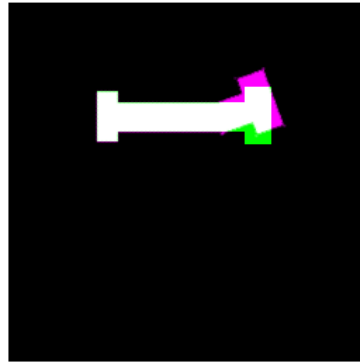


Figure 5.8: Proximal image registration. The pink represents the deformed bone and the green represents the reference bone. White represents the area where the two bones overlap.

When performing these image registrations on the two bones, it is especially important to keep track of the second registration. The geometric transform from distal alignment to proximal alignment will provide information needed for the reconstruction of the deformed bone. In order to do this, a spatial referencing object is created for each image. This keeps track of where in space the image is located and is particularly useful for the cropped images used for the distal and proximal registration. For two dimensions the spatial referencing object is created with the function `imref2d` which stores information about the relation between the image coordinates and the world coordinates. The world coordinates can be defined by the original image size as a default. If the image is cropped the spatial referencing object belonging to the cropped image can be updated so that the information about its relation to the original image is kept. By having a spatial referencing object referring to each image, a geometric transform can be computed for a cropped image but applied to the full size image using the `imwarp` function. This will keep computational time for the image registration down as well as giving the user, i.e. the developer or the surgeon planning the surgical procedure, the option of deciding how much of the distal or proximal end of the bone that is desired to be matched to the reference. This can be useful if there is an anatomical difference between the two bones, for instance caused by the fracture.

5.2.2 Reconstruction process

When both the distal and the proximal ends are aligned to the reference image and any manual post registration adjustments have been made, the geometric transform for the second alignment is stored.

The next step is to plan the surgical cut. The position of the cut is marked and the image is divided in two at this mark. The two parts of the image is then moved to each end's prior alignment from the image registration, see Figure 5.9. This is done by applying the geometric transform to each of the image parts. The resulting reconstruction is evaluated and if not satisfactory, the cut is repositioned and the reconstruction process is performed again.

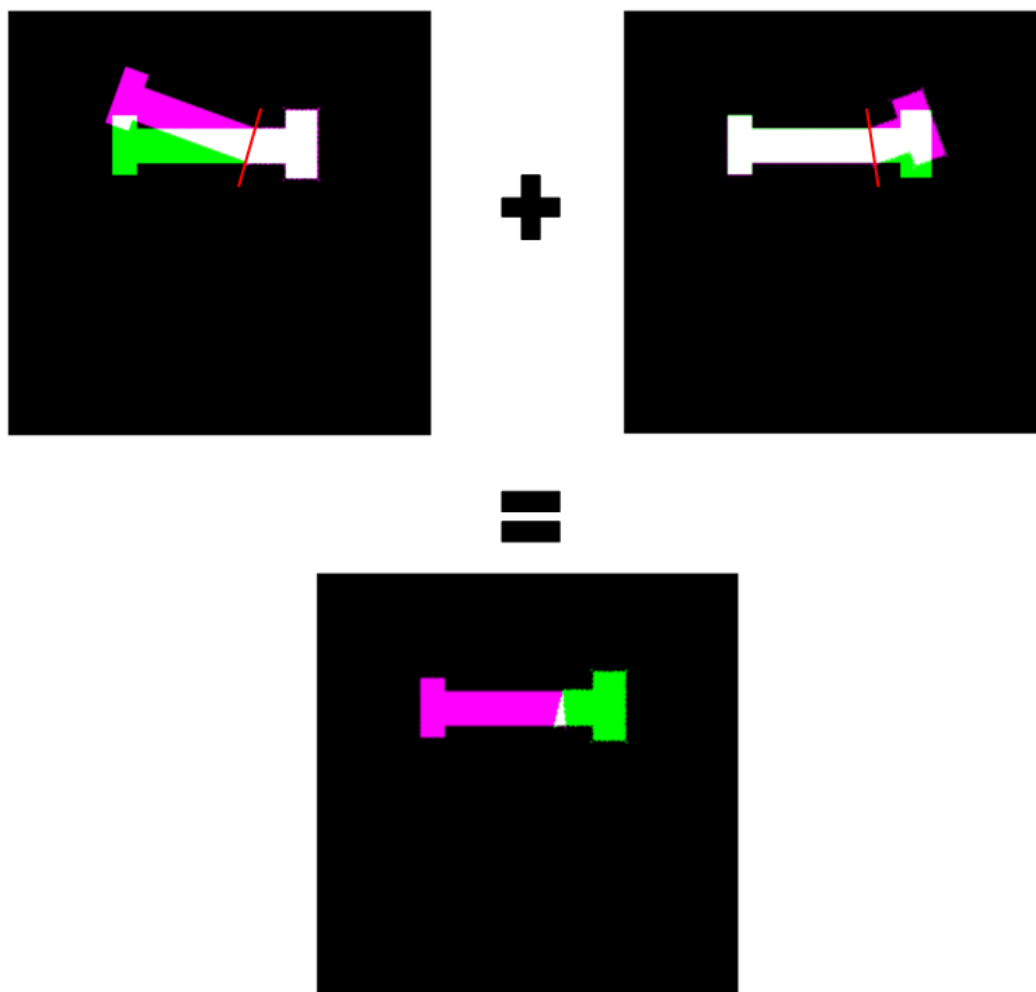


Figure 5.9: Reconstruction step for two dimensional test case. The red lines represent placement of the cut, the white part of the bottom image represents overlap meaning there is a collision of the two image parts.

5.3 Three dimensional reconstruction

The expansion of the reconstruction process to three dimensions is rather trivial. Now there will be rotation about three axes instead of just one and translation along three axes instead of two. The functions used for the two dimensional test case has versions for three dimensions as well.

5.3.1 Aligning process

The reconstruction process is the same for three dimensions as explained for the two dimensional test case. A prior step however is to mirror the healthy contralateral radius bone in the sagittal plane in the Segment 3DPrint software. This gives the reference bone for the reconstruction process. The vertex coordinates of the reference and deformed bone is converted from Segment 3DPrint coordinates to patient coordinates and loaded into the Planningtool software. The deformed bone, the malunited radius, is aligned distally and proximally to the reference bone in the same two step registration process as for the two dimensional test case. The first step consisting of selecting how much of the distal end of the deformed radius that is to be registered to the reference radius. For visual aid in the decision, a cut plane is placed on the bone. This plane can be moved and rotated and when the user is satisfied with its location the two images are cropped and the deformed part is registered to the reference part. The geometric transform from this registration is applied to the deformed bone and stored as a new object, see step 3 in Figure 5.10.

With the distally aligned deformed bone, the same procedure is done on the proximal ends of the deformed and reference radius, see step 3-4 in Figure 5.10. After the second registration there will be two copies of the deformed bone, one with the distal alignment applied and one with the proximal alignment applied as shown in step 6 in Figure 5.10. The next step is the reconstruction of the deformed bone, the cut plane is placed along either of the aligned copies, as a suggestion where the two exhibits the most overlap, and this copy is cut, step 6-8 in Figure 5.10, and the end that is not aligned is transformed using the alignment for the other copy. In Figure 5.10 the distally aligned copy is cut and the proximal end is aligned using the geometric transform from the second registration, step 8-9. If one were to instead cut the proximally aligned copy, the distal end will be aligned using the inverse of the geometric transform from the second registration. The cut plane coordinates are stored for placement of the slit on the cutting guide. The reconstruction may be adjusted manually if needed, see step 10-11 in Figure 5.10.

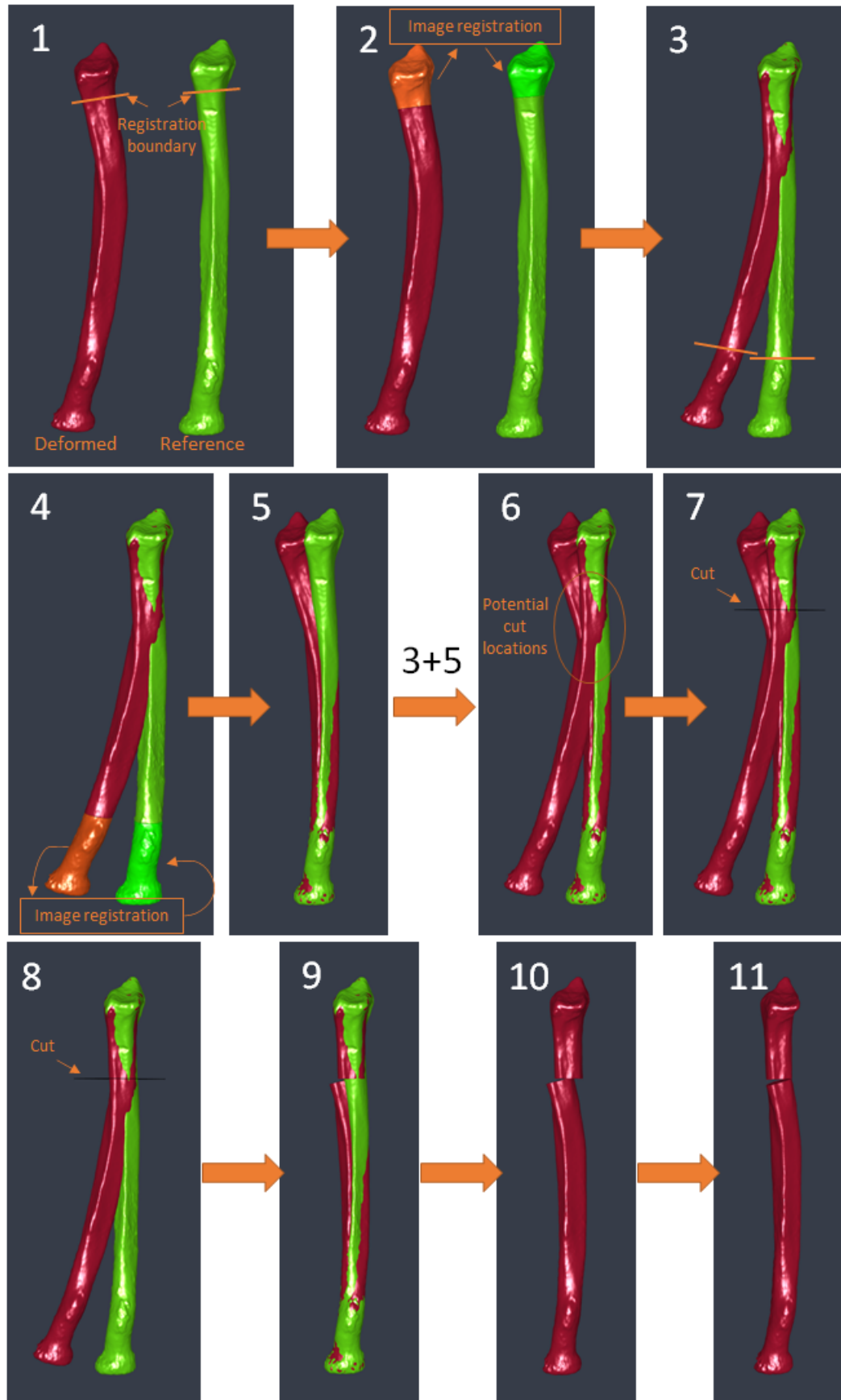


Figure 5.10: Flow chart of the reconstruction process for three dimensions. Red is the deformed bone, green is the mirrored reference bone.

5.3.2 Plate placement

When the deformed bone is cut and aligned both distally and proximally a model of the fixation plate is loaded into the software. There are currently two plate models implemented and one of them, the NLP, is available for use but the idea is to eventually have a catalogue of different plate models to choose from. The sample plates were provided by Anders Björkman. One plate, a DVR plate from DePuy Synthes, was scanned with a ATOS I SO made by GOM. For the second plate, a straight NLP (non locking plate), a CAD model (computer-aided design) were provided by Philip Bernborg, Bild & Funktionsteknik, Skåne University Hospital, Lund.

If the plate cannot be placed with a satisfactory fit onto the reconstructed bone, the alignment may be manually adjusted as the user deems appropriate. If the cut location from the reconstruction step is deemed unfit, this step (step 7 in Figure 5.10) can be performed again with a different placement of the cut plane. When a satisfactory placement is found the transforms for each part of the reconstructed bone are updated. The inverse of the geometric transform between the two parts is computed in order to find corresponding coordinates for the plate holes on the original deformed bone.

5.4 3D model of a surgical cutting guide

When the surgical plan is created, the inverse transformed plate hole coordinates are converted to Segment 3DPrint coordinates. These coordinates will be input for the drill guides on the cutting guide. The user may decide diameter of the drill guide as well as the thickness of the drill guide walls. The base plate of the cutting guide is created by modifying an already existing function in the Segment 3DPrint software for text labels. This function follows the curvature of the object and creates a label between chosen points. For the cutting guide these points will be decided from the placement of the plate, the end holes will give the length needed of the base plate. The cut location from the reconstruction step is converted to Segment 3DPrint coordinates and decides the center placement of the slit, the user may decide its width. The base plate, drill guides and slit are merged into one object, creating the cutting guide. The deformed bone is subtracted from the cutting guide to take care of possible collisions between the two. This will create a cutting guide that fits exactly to the bone.

For distal radius malunions the base of the cutting guide may be extended towards the watershed line (marked in Figure 5.2) on the bone to improve the fit of the cutting guide. When the reconstruction cut is located closer to the proximal end of the radius this may not be an option due to limitations in the desire to not place an incision much larger than the fixation plate used.

Chapter 6

Results

From the explained methodology, functions that extend the possibilities in the Segment 3DPrint software have been implemented. These functions and methods enable the creation of the first cutting guides for radius malunions.

The results from distal and proximal alignment using intensity based image registration are presented for all three patient cases. A proposed reconstruction of patient C is presented in Chapter 6.3 together with a cutting guide. Proposed reconstructions of patient A and patient B is presented in Appendix A and B, respectively. The suggested plate placement from the reconstructions for patient A and patient B is included in the results below for evaluation purposes.

6.1 Patient A

The proximal and distal alignments from the registration process for patient A can be seen in Figure 6.1. The distal alignment shows a good fit of the articular surface.



Figure 6.1: Patient A alignment (right radius malunion), dark grey is the mirrored reference bone, light grey is the deformed radius.

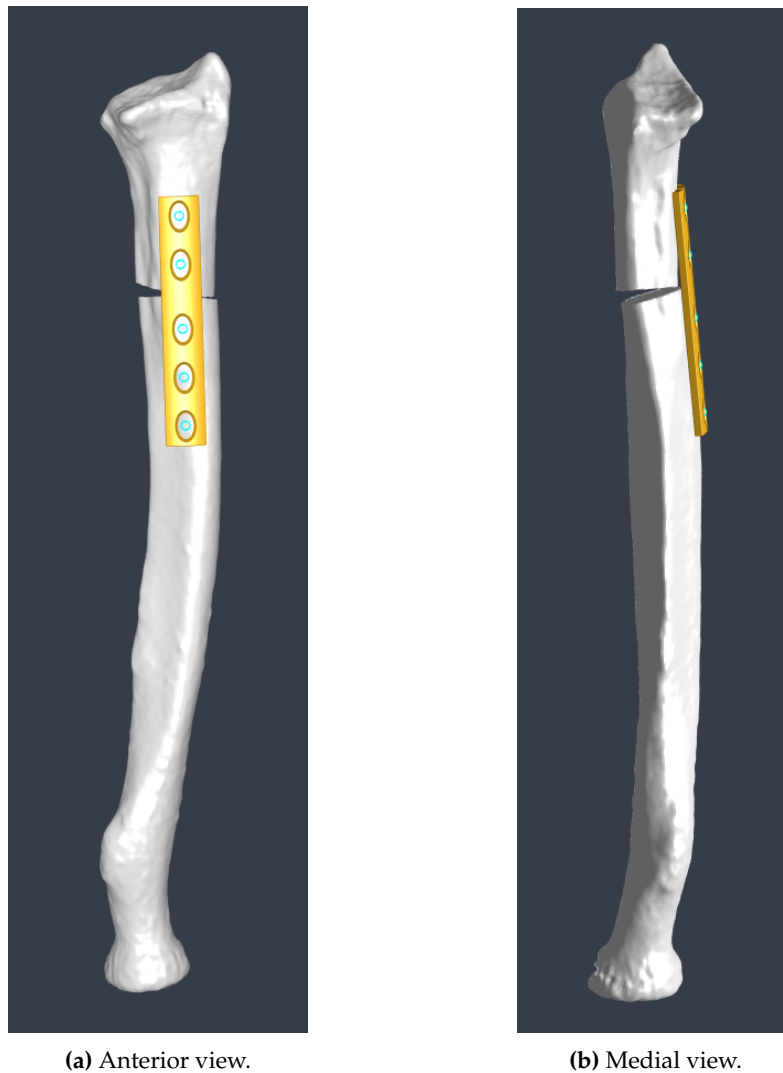


Figure 6.2: Patient A plate placement (right radius malunion).

The suggested plate placement after reconstruction is seen in Figure 6.2. In the medial view a slight distance between the plate and the anterior surface of the bone exists between the cut location and the closest plate hole on the distal part.

6.2 Patient B

The alignments from the registration process for patient B are presented in Figure 6.3. The distal alignment shows a good fit for the articular surface, however the proximal alignment does not completely fit the articular surface of the reference bone. An additional proximal registration was performed using a registration boundary below the radial tuberosity. The resulting alignment is presented in Figure 6.4, showing a slightly better fit of the articular surface but more lateral rotation of the radial tuberosity compared to the initial alignment. Results for the articular surface alignment with the initial registration boundary can be seen in Appendix B.



Figure 6.3: Patient B alignment (right radius malunion), dark grey is the mirrored reference bone, light grey is the deformed radius.

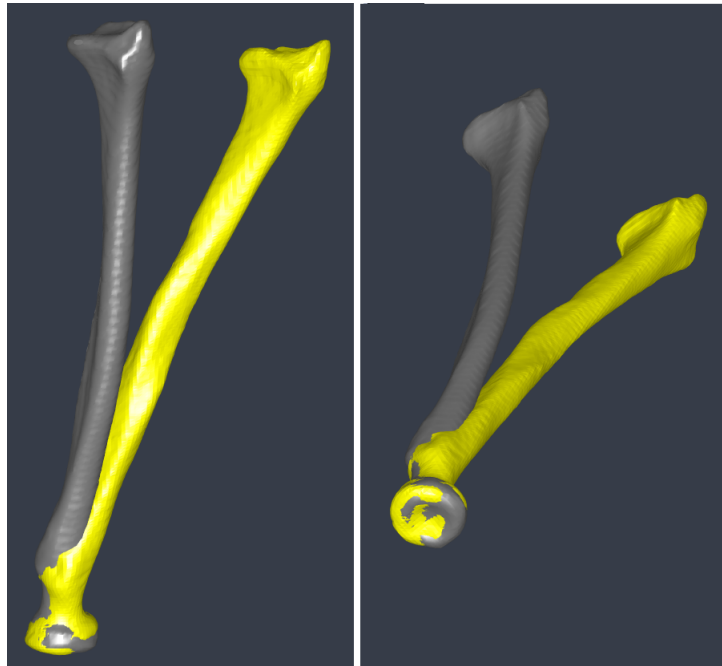


Figure 6.4: Patient B, proximal alignment using a registration boundary below the radial tuberosity.

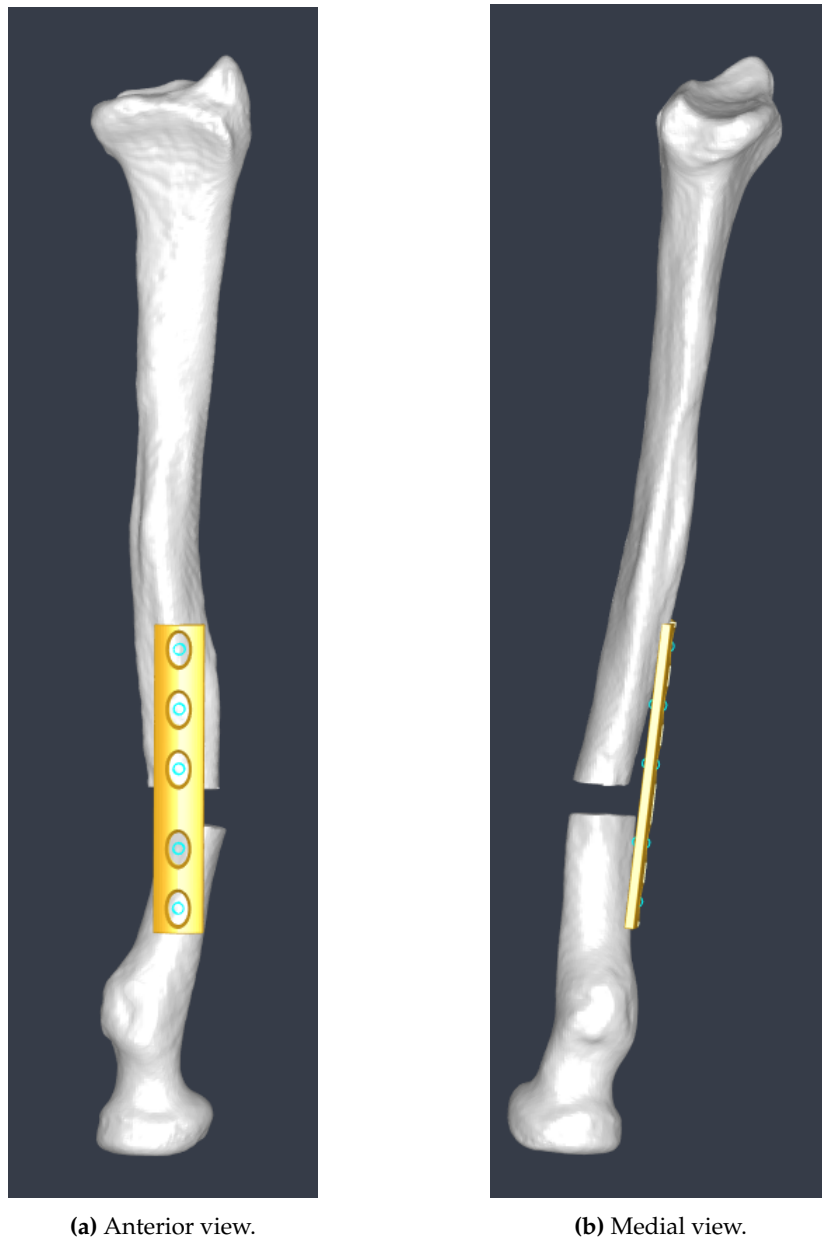


Figure 6.5: Patient B plate placement (right radius malunion).

The suggested plate placement after reconstruction is seen in Figure 6.5. The anterior view shows a shape of the reconstructed bone that makes it somewhat difficult to achieve a good plate placement. The medial view shows distance between the plate and the anterior surface of the bone on both sides of the cut. The reconstruction for patient B also gives rise to a significant gap between the distal and proximal parts.

6.3 Patient C

The alignments from the registration process for patient C are presented in Figure 6.6. Both alignments shows a good fit for the articular surfaces, see fit for the proximal articular surface in Figure 6.8c.



Figure 6.6: Patient C alignment (left radius malunion), dark grey is the mirrored reference bone, light grey is the deformed radius.

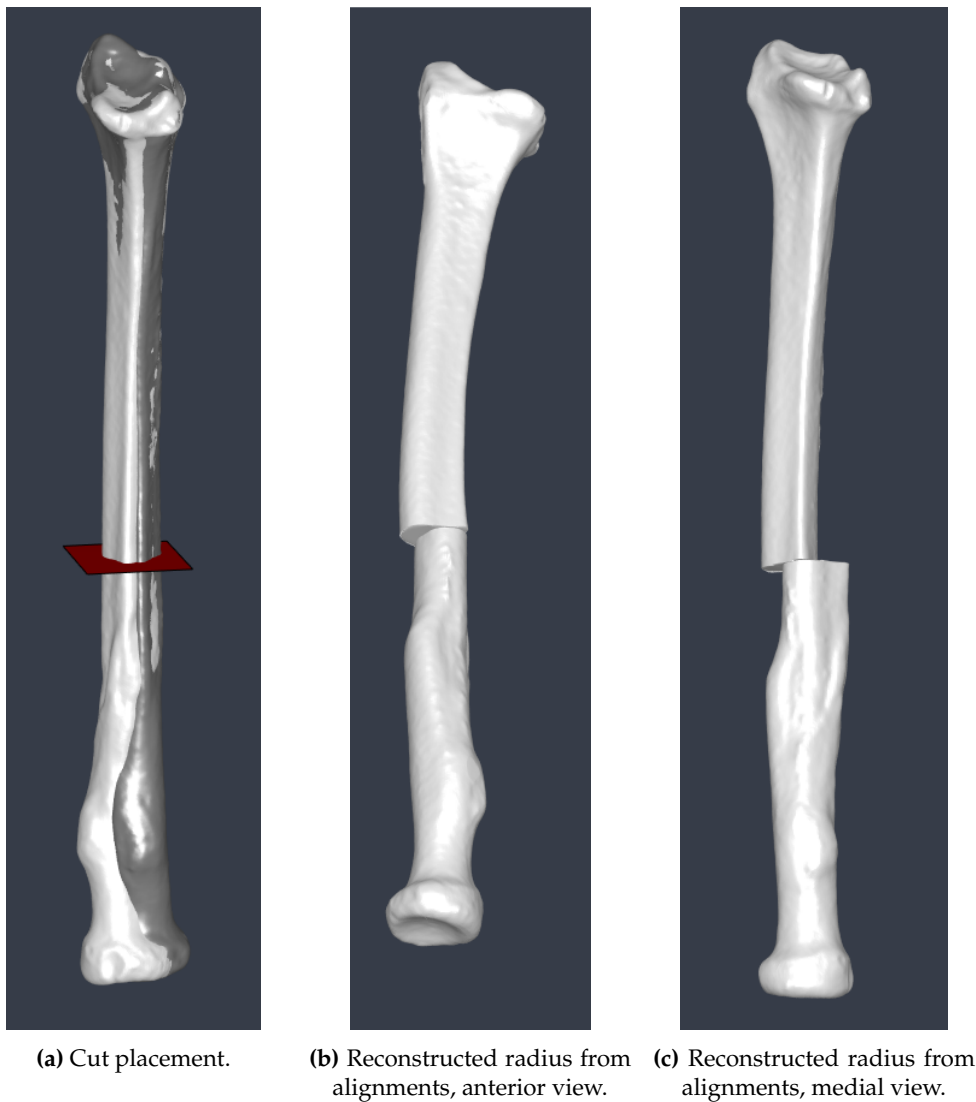


Figure 6.7: Patient C reconstruction process (left radius malunion), dark grey is the mirrored reference bone, light grey is the deformed radius.

The cut plane, red in Figure 6.7a, was placed in close proximity of the fracture site as well as where the overlap of the distally and proximally aligned bone was good, i.e. if Figure 6.6b and 6.6a were to be put on top of each other. The reconstructed radius using the alignment from the registration is shown in Figure 6.7b and 6.7c.



(a) Reconstructed radius with manual adjustments, anterior view. (b) Reconstructed radius with manual adjustments, medial view. (c) Comparison to reference.

Figure 6.8: Patient C reconstruction process (left radius malunion), dark grey is the mirrored reference bone, light grey is the deformed radius.

Some minor manual adjustments was made to shift the proximal part laterally to find a surface matching the curvature of the distal part, see Figure 6.8a and 6.8b. These adjustments included translation (both anterior-posterior and medial-lateral) and rotation (medial-lateral and anterior-posterior). The reference bone is included in Figure 6.8c to ensure a good fit for the proximal articular surface.



Figure 6.9: Patient C plate placement (left radius malunion).

The suggested plate placement is presented in Figure 6.9. Some distance between the plate and the proximal part can be seen in the lateral view. A small overlap between the two parts can also be seen in the lateral view.

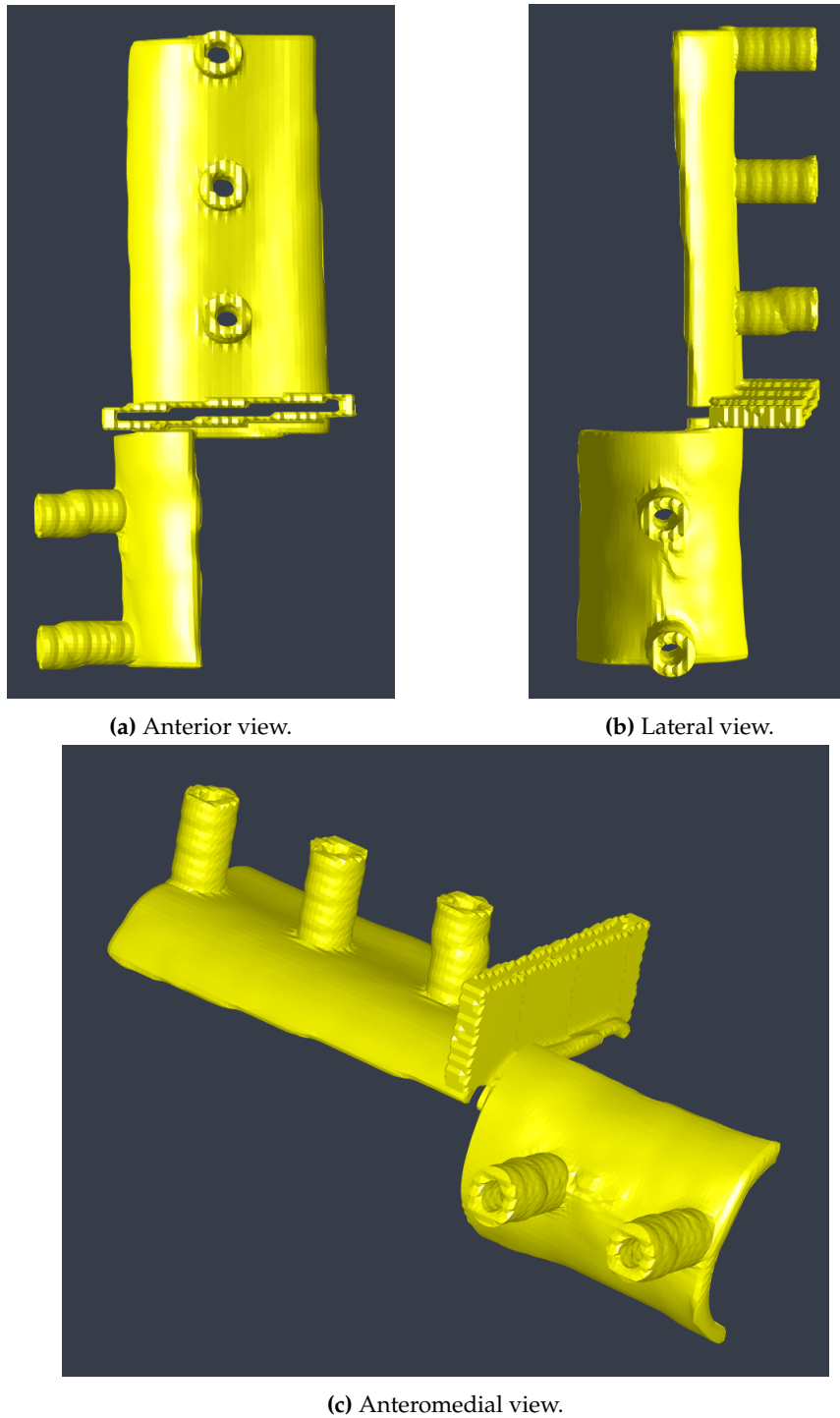


Figure 6.10: Patient C cutting guide (left radius malunion).

The resulting cutting guide from the final alignments is presented in Figure 6.10 and its placement on the deformed radius can be seen in Figure 6.11. A cutting guide typically has smaller holes for fixating the plate to the bone with wires prior to the cut, however such holes have not been added to the cutting guide models for this project.

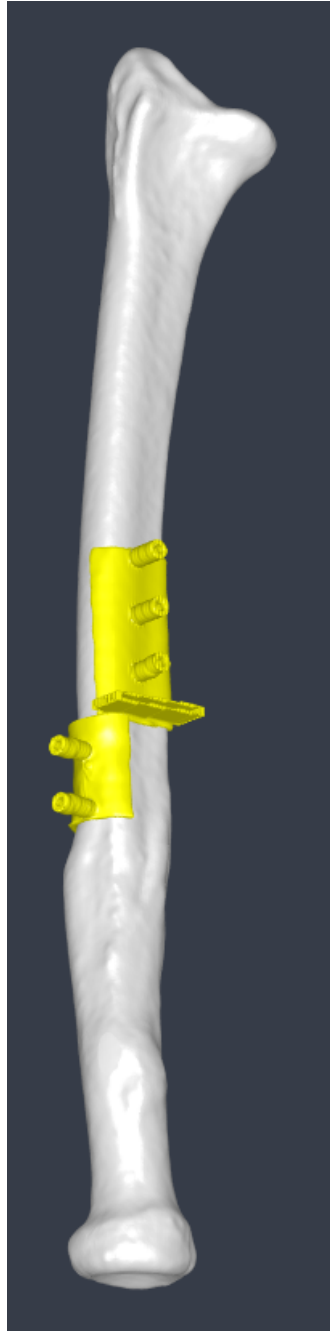


Figure 6.11: Patient C cutting guide placement on deformed left radius.

Chapter 7

Discussion

To summarise, the accomplished content of this master thesis are the following. Development of two dimensional phantoms to test the intended methodology of the software. Modifying the Segment 3DPrint software to support construction of the cutting guides. Performing experiments on three dimensional patient cases to further improve the surgical planning tool.

Ideally one would like to formulate the creation of the cutting guide and the placement of the cut as an optimisation process. This was the starting aim for the project but was deemed to be difficult and too challenging as there might be surgical constraints on where a cut can be placed. These constraints may even differ between patients and implementing them as general constraints may not be possible. A surgical incision closer to the distal part of the forearm is generally preferred due to an increasing amount of muscle tissue towards the proximal part. In some cases a distal incision can be proven difficult if the fracture site is located on the proximal part, as the deformity often arises close to the fracture site. An optimisation for the cut placement can of course give a good initial suggestion and could for example be implemented as maximising the dice score, see formula in (5.1), in the transverse view of the distally and proximally aligned bones.

Since the deformed bone is registered to the reference bone which is the healthy contralateral radius bone, there may be some local mismatching due to the fact that both radiuses are not completely identical. This is illustrated in the proximal alignment for patient B, Figure 6.3a, where the radial tuberosity differs between the two bones enough for the alignment in the proximal articular surface to be affected. One could set the proximal registration boundary to not include the radial tuberosity in order to improve alignment in the articular surface. An issue with this however is the symmetry of the radial head which may lead the optimisation algorithm to reach a minimum with a large rotation error. As the results show in Figure 6.4, this rotation error is small and the alignment in the proximal articular surface is better. However the problem arises with finding a cut location where the distally and proximally aligned bone parts can provide a surface for the fixation plate to be placed upon. This shows that for some cases there may be a trade off in the alignments in order to create a satisfactory surface for the plate placement. Another possibility to improve this surface is to place an additional cut on the bone. As seen in Figure B.4 the shape of the reconstructed bone makes it difficult for plate placement. An additional cut on the distal part may result in a closer fit to the bone surface, however depending on the location of this additional cut, a longer plate may be required in order to get enough fixation points per bone part.

When a distal incision is possible, as for patient A shown in Figure A.6, it may be of interest to extend the exposed bone toward the watershed line as mentioned in Chapter 5.4 to improve the fit of the cutting guide. This also allows the usage of a DVR plate which is anatomically designed for the distal radius. If a DVR was to be used for patient A it would probably be a longer one than shown in Figure 2.4b since the cut is located too far from the distal end for the regular DVR plate. For the interested reader plate placement using the DVR for patient A can be seen in Appendix A.

Regarding large rotational deformations, as for patient C shown in Figure 6.6a, the resulting cutting guide will wrap around the deformed bone for approximately 90 degrees. This will require a large incision as well as a large exposure of the bone. It may be difficult to place the cutting guide in the incision, since the cut is placed in the middle of the bone there will be quite a bit of muscle tissue that will need to be detached and moved. A possible solution is to create multiple guides, one for the saw slit and one for the drill guides. This will allow the surgeon to first cut and rotate the bone and then drill the holes for the fixation plate. This will require the two guides to have holes for the fixation wires to be placed strategically in order to compensate for the rotation of the bone between the cut and the drilled holes. This to ensure that the second guide will have the correct placement on the bone. Furthermore, the collision seen in the reconstruction for this patient needs attending, see Figure 6.9b. This can either be fixed freehand by the surgeon during the surgery or by placing a second saw slit close to the first one. This will remove a small piece of bone and give space for the two bone parts in the reconstruction.

7.1 Limitations

There are several limitations in the current implementation that will need to be considered before the planning tool can be used clinically. The limitations in the tool are:

- The software only supports one cut.
- Only one plate can be used.
- No adjustments possible on optimisation parameters for the user as these are hard coded. Some registrations may take long to converge to an optimum.

7.2 Future work

Future work should of course be to test the cutting guides and validate the success of the osteotomy, unfortunately the development of the software and algorithms were too extensive in order to reach the point where testing and validation could be carried out. Other important future work is to continue developments of the software and improve plate generation, support for fixation wires on the guides, implement function to snap plates to the bone surface and provide higher resolution of the final cutting guides.

An interesting expansion for the program would be to include a shape model of a radius. This would make it possible to use the software to create cutting guides for patients that do not have a healthy contralateral radius to use as a reference.

Chapter 8

Conclusions

This master thesis has implemented tools necessary to create the first proof-of-concept cutting and drilling guides for radius malunion. The software developed during this master thesis is very much a work in progress. There are some desired features yet to be implemented and at its current state it works more as a planning environment that gives a good overview of the deformed bone. With that said, the ultimate aim to create surgical cutting guides on site at the hospital was not reached at the end of this project.

However, the program provides the ability to rotate, translate and cut objects and using the performed transformations to reconstruct a deformed bone. The idea to locate the cut placement using mathematical optimisation was abandoned due to limitations with surgical constraints.

Bibliography

- [1] Michael Schuenke et al. *Atlas of Anatomy Image Collection*. Thieme Publishing Group, 2006.
- [2] Laura E Diment, Mark S Thompson, and Jeroen H M Bergmann. "Clinical efficacy and effectiveness of 3D printing: a systematic review". In: *BMJ Open* 7.12 (2017). Available from: <https://bmjopen.bmj.com/content/7/12/e016891>, [Accessed 27-January-2020]. ISSN: 2044-6055. DOI: 10.1136/bmjopen-2017-016891. eprint: <https://bmjopen.bmj.com/content/7/12/e016891.full.pdf>. URL: <https://bmjopen.bmj.com/content/7/12/e016891>.
- [3] D. H. Ballard et al. "Medical 3D Printing Cost-Savings in Orthopedic and Maxillofacial Surgery: Cost Analysis of Operating Room Time Saved with 3D Printed Anatomic Models and Surgical Guides". In: *Acad Radiol* (2019).
- [4] R. K. Card and J. B. Lowe. *Anatomy, Shoulder and Upper Limb, Elbow Joint*. Available from: <https://www.ncbi.nlm.nih.gov/books/NBK532948/>, [Accessed 27-January-2020]. Treasure Island (FL): StatPearls Publishing, [Updated 2019 Jan 16].
- [5] J. Erwin and M. Varacallo. *Anatomy, Shoulder and Upper Limb, Wrist Joint*. Available from: <https://www.ncbi.nlm.nih.gov/books/NBK534779/>, [Accessed 27-January-2020]. Treasure Island (FL): StatPearls Publishing, [Updated 2-December-2018].
- [6] R. A. Berger. "The anatomy and basic biomechanics of the wrist joint". In: *J Hand Ther* 9.2 (1996), pp. 84–93.
- [7] J. E. Adams. "Forearm Instability: Anatomy, Biomechanics, and Treatment Options". In: *J Hand Surg Am* 42.1 (2017), pp. 47–52.
- [8] J. T. Helms, K. A. Maldonado, and B. Burns. *Anatomy, Shoulder and Upper Limb, Hand Radiocarpal Joint*. Available from: <https://www.ncbi.nlm.nih.gov/books/NBK539744/>, [Accessed 01-June-2020]. Treasure Island (FL): StatPearls Publishing, [Updated 11-April-2020].
- [9] G Lundborg and A Bjorkman. *Handkirurgi*. Illustrations by: Johansson, F. Studentlitteratur, 2015.
- [10] M. Soubeyrand et al. "Pronation and supination of the hand: Anatomy and biomechanics". In: *Hand Surg Rehabil* 36.1 (2017), pp. 2–11.
- [11] BT Evans and JB Jupiter. "Best Approaches in Distal Radius Fracture Malunions". In: *Curr Rev Musculoskelet Med* 12.2 (2019), pp. 198–203. DOI: 10.1007/s12178-019-09540-y.
- [12] Thomas G. Wadsworth. "Colles' Fracture: Failure In Management May Cause Permanent Disability". In: *BMJ: British Medical Journal* 301.6745 (1990). Available from: <http://www.jstor.org/stable/29708565>, [Accessed 27-January-2020], pp. 192–194. ISSN: 09598138, 17561833. URL: <http://www.jstor.org/stable/29708565>.

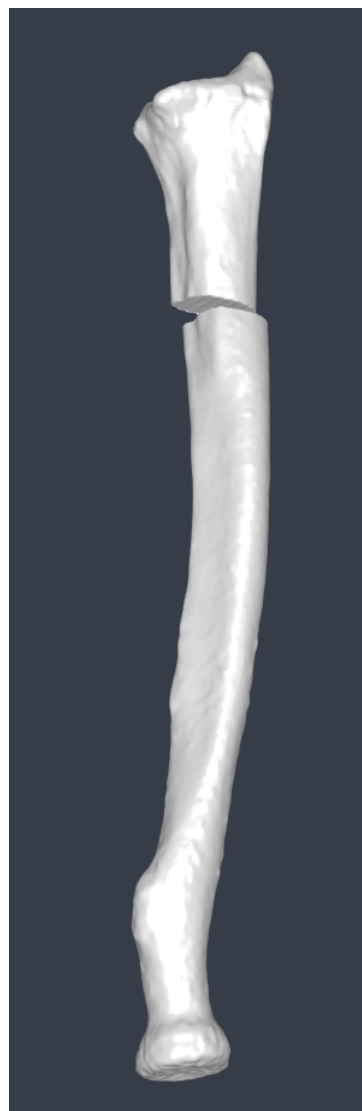
- [13] Johns Hopkins Medicine. *Surgical Site Infections*. [Online; accessed 09-June-2020]. 2020. URL: [\url{https://www.hopkinsmedicine.org/health/conditions-and-diseases/surgical-site-infections}](https://www.hopkinsmedicine.org/health/conditions-and-diseases/surgical-site-infections).
- [14] H. Cheng et al. "Prolonged Operative Duration Increases Risk of Surgical Site Infections: A Systematic Review". In: *Surg Infect (Larchmt)* 18.6 (2017). Available from: <https://www.ncbi.nlm.nih.gov/pmc/articles/PMC5685201/>, [Accessed 09-June-2020], pp. 722–735.
- [15] C. L. Ventola. "Medical Applications for 3D Printing: Current and Projected Uses". In: *P & T : a peer-reviewed journal for formulary management* 39.10 (2014), pp. 704–711.
- [16] G. Song et al. "A Review on Medical Image Registration as an Optimization Problem". In: *Curr Med Imaging Rev* 13.3 (2017), pp. 274–283.
- [17] MathWorks. *Image Processing Toolbox User's Guide*. English. Version Version 11.0. Chapter 7, Available at: <https://se.mathworks.com/help/images/index.html>, [Accessed 30-January-2020]. MathWorks. 1642 pp. Forthcoming.
- [18] MathWorks. *Image Processing Toolbox User's Guide*. English. Version Version 11.0. Chapter 6, Available at: <https://se.mathworks.com/help/images/index.html>, [Accessed 30-January-2020]. MathWorks. 1642 pp. Forthcoming.
- [19] MathWorks. *Computer Vision Toolbox User's Guide*. English. Version Version 9.1. Chapter 9, Available from: <https://se.mathworks.com/help/vision/index.html>, [Accessed 20-February-2020]. MathWorks. 554 pp. Forthcoming.
- [20] Wikimedia Commons Cmglee. *File:Comparison of 1D and 2D interpolation.svg — Wikimedia Commons, the free media repository*. [Online; accessed 20-March-2020]. 2016. URL: [\url{https://commons.wikimedia.org/w/\index.php?curid=53064904}](https://commons.wikimedia.org/w/\index.php?curid=53064904).
- [21] D. L. Hill et al. "Medical image registration". In: *Phys Med Biol* 46.3 (2001), pp. 1–45.
- [22] J. Nocedal and S. J. Wright. *Numerical Optimization*. Springer Science & Business Media, 2006.
- [23] MathWorks. *Image Processing Toolbox Reference*. English. Version Version 11.0. Chapter 1 p. 2491, Available at: <https://se.mathworks.com/help/images/index.html>, [Accessed 30-January-2020]. MathWorks. 3440 pp. Forthcoming.
- [24] H. D. Tagare and M. Rao. "Why Does Mutual-Information Work for Image Registration? A Deterministic Explanation". In: *IEEE Transactions on Pattern Analysis and Machine Intelligence* 37.6 (2015), pp. 1286–1296.
- [25] MathWorks. *Image Processing Toolbox Reference*. English. Version Version 11.0. Chapter 1 p. 2182, Available at: <https://se.mathworks.com/help/images/index.html>, [Accessed 30-January-2020]. MathWorks. 3440 pp. Forthcoming.
- [26] Smriti Raghunathan et al. *Image Registration Using Rigid Registration and Maximization of Mutual Information*. Poster presented at: MMVR13. The 13th Annual Medicine Meets Virtual Reality Conference, 26-29-January-2005, Long Beach, CA, [Accessed 10-June-2020]. 2005. URL: [\url{https://www.osc.edu/files/research/Biomed/vtbone/updates/image_registration.pdf}](https://www.osc.edu/files/research/Biomed/vtbone/updates/image_registration.pdf).

Appendix A

Results patient A



(a) Cut placement, medial view.



(b) Reconstructed radius from alignments, anterior view.

Figure A.1: Patient A reconstruction process (right radius malunion), dark grey is the mirrored reference bone, light grey is the deformed radius.

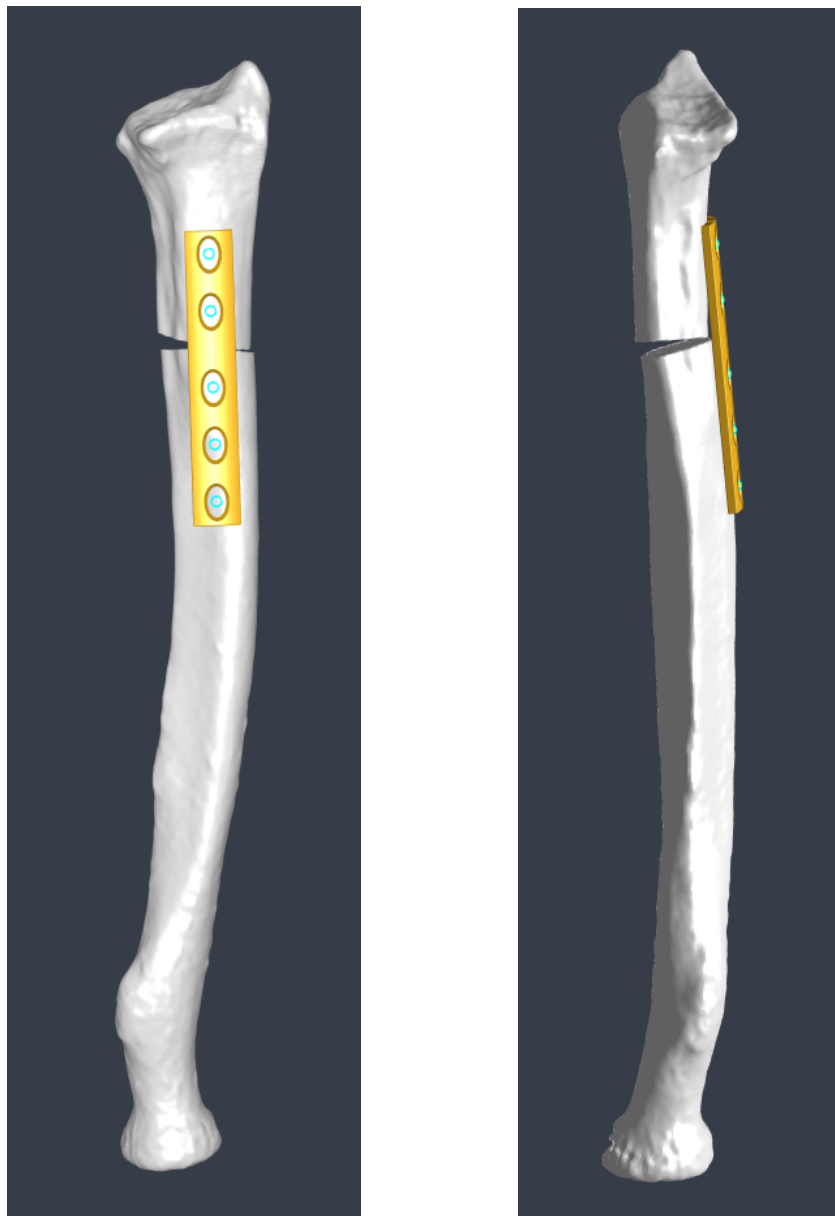


(a) Reconstructed radius with manual adjustments, anterior view.



(b) Comparison to reference.

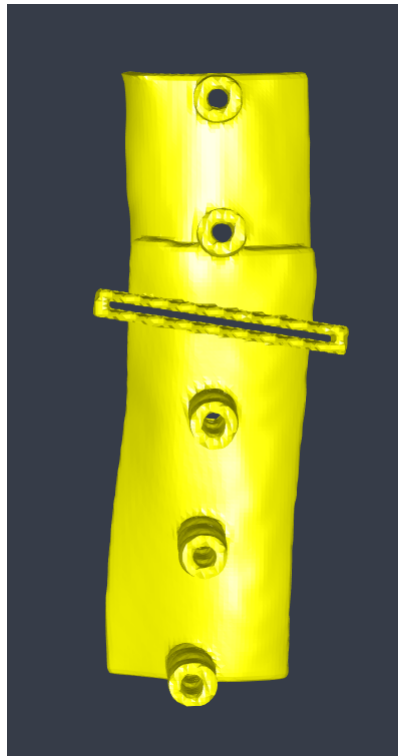
Figure A.2: Patient A reconstruction process (right radius malunion), dark grey is the mirrored reference bone, light grey is the deformed radius.



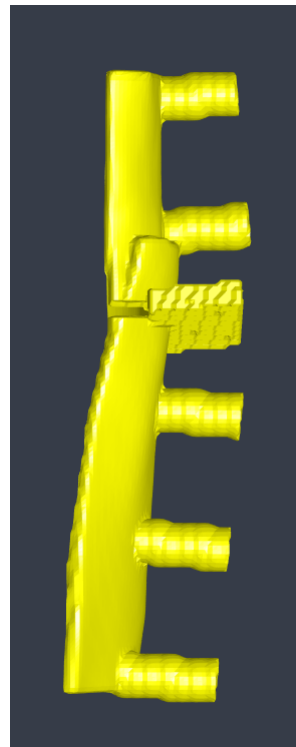
(a) Anterior view.

(b) Medial view.

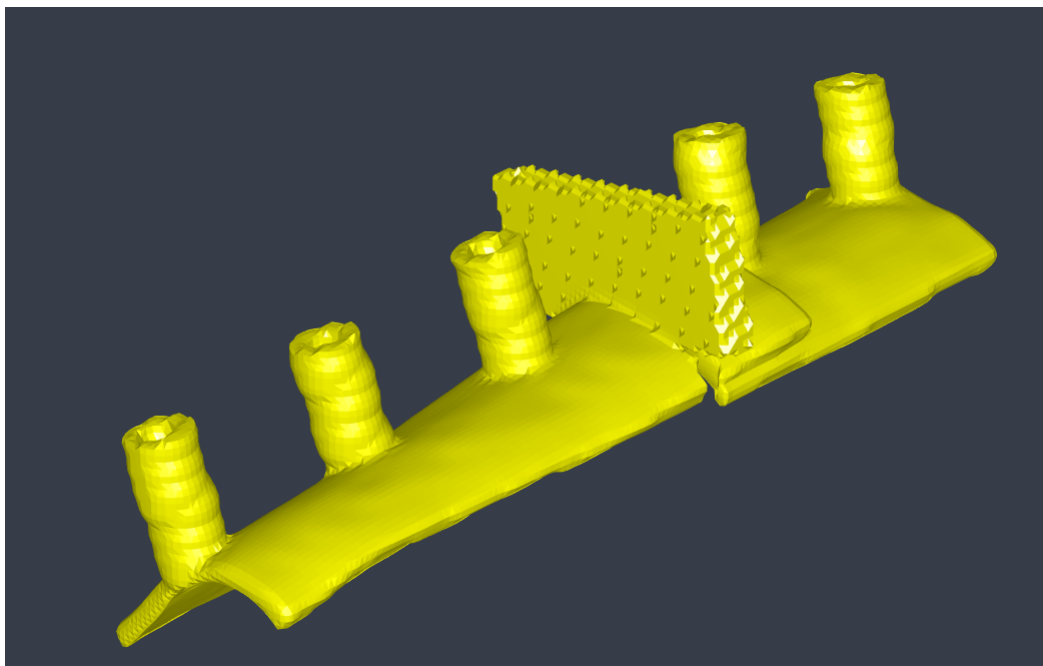
Figure A.3: Patient A plate placement (right radius malunion).



(a) Anterior view.



(b) Medial view.



(c) Anterolateral view.

Figure A.4: Patient A cutting guide (right radius malunion).



Figure A.5: Patient A cutting guide placement on deformed right radius.

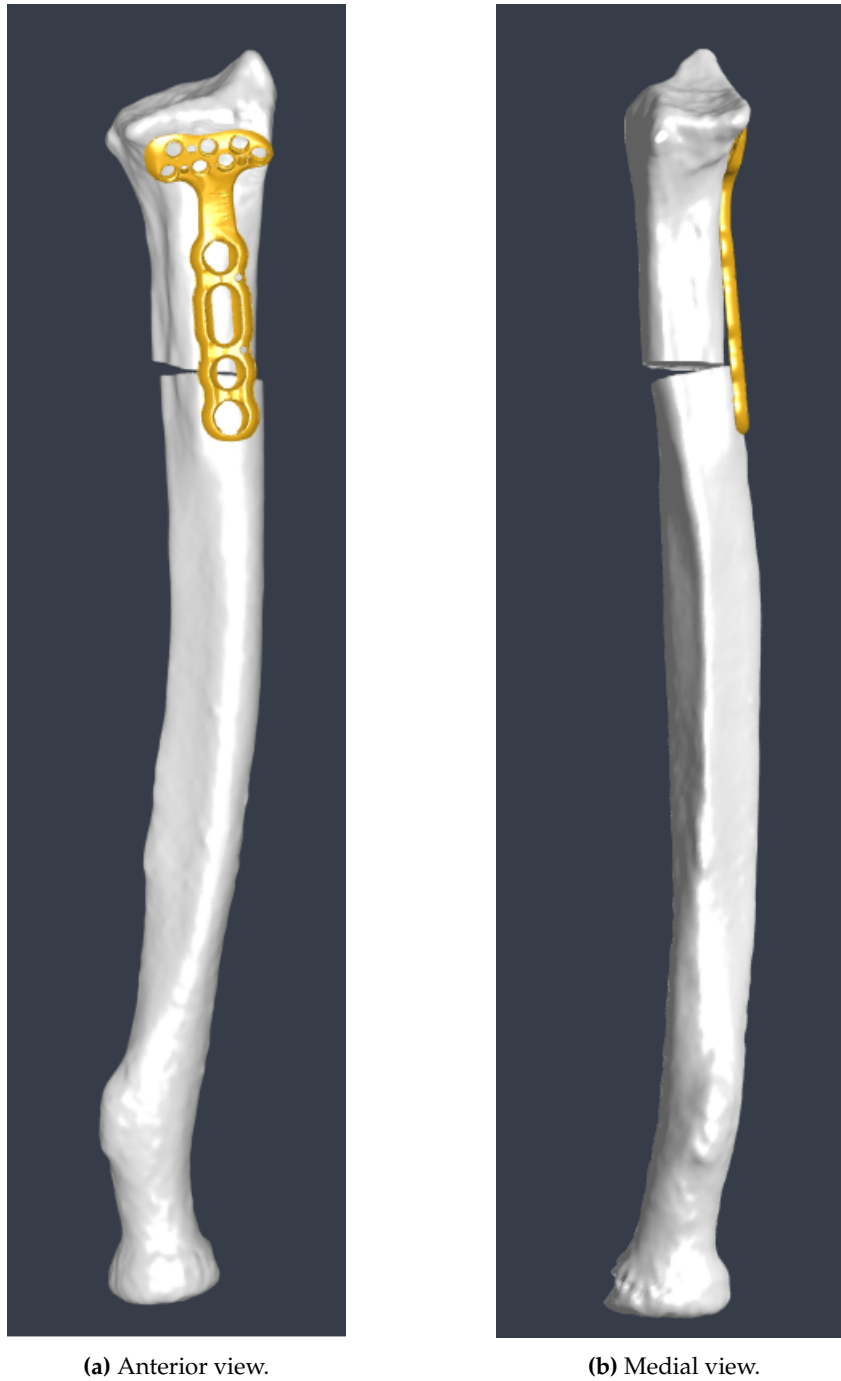
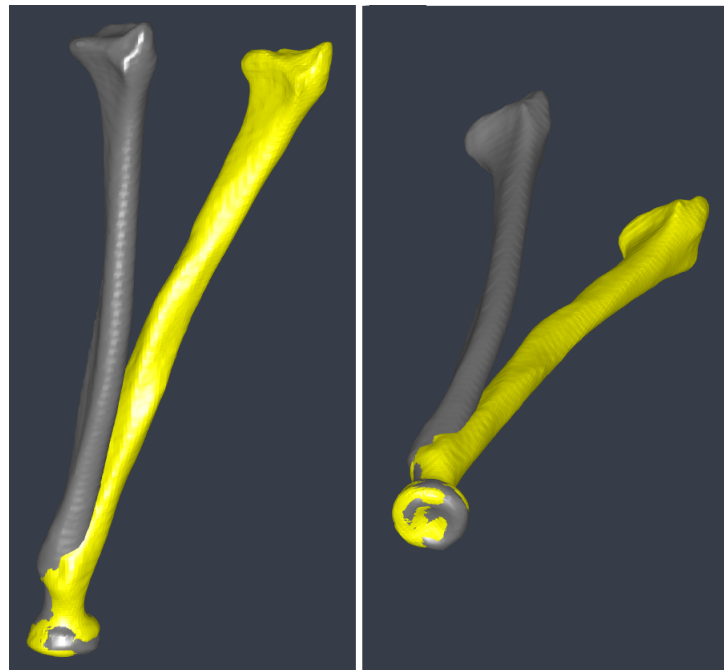


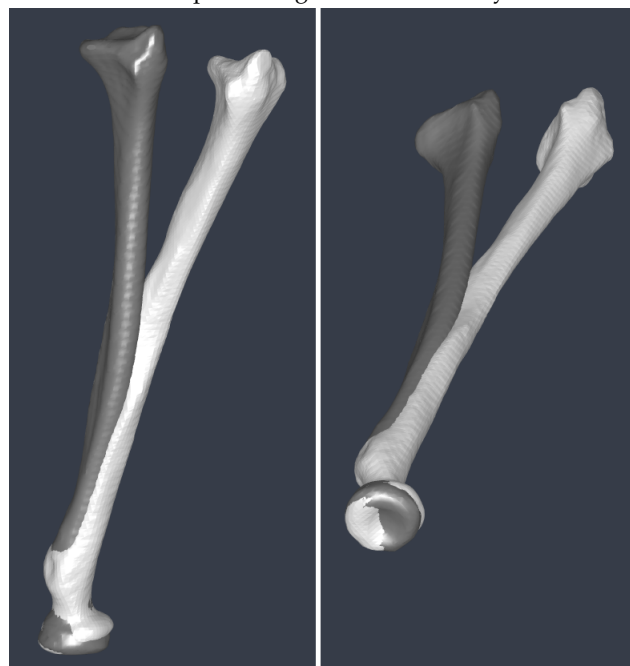
Figure A.6: Patient A plate placement using the DVR plate (right radius malunion).

Appendix B

Results patient B



(a) Optional registration boundary.



(b) Registration boundary above tuberosity.

Figure B.1: Patient B, proximal alignment with registration boundary below the radial tuberosity compared to boundary above the radial tuberosity.



(a) Cut placement, anterior view. (b) Reconstructed radius from alignments, anterior view. (c) Reconstructed radius from alignments, medial view.

Figure B.2: Patient B reconstruction process (right radius malunion), dark grey is the mirrored reference bone, light grey is the deformed radius.

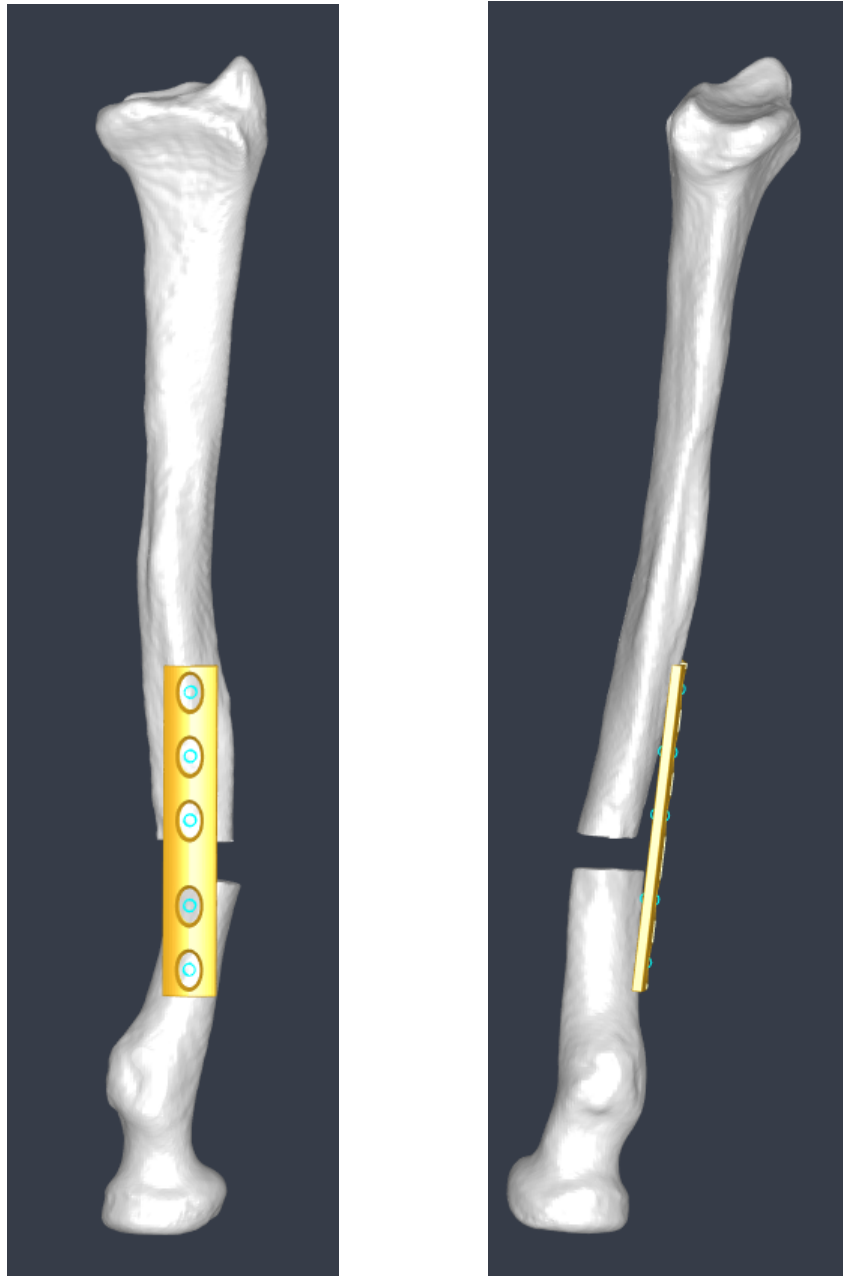


(a) Reconstructed radius with manual adjustments, medial view.



(b) Comparison to reference.

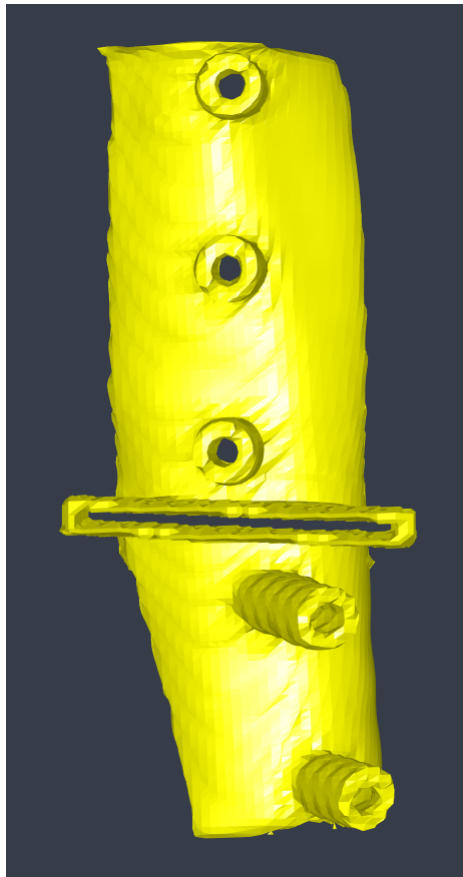
Figure B.3: Patient B reconstruction process (right radius malunion), dark grey is the mirrored reference bone, light grey is the deformed radius.



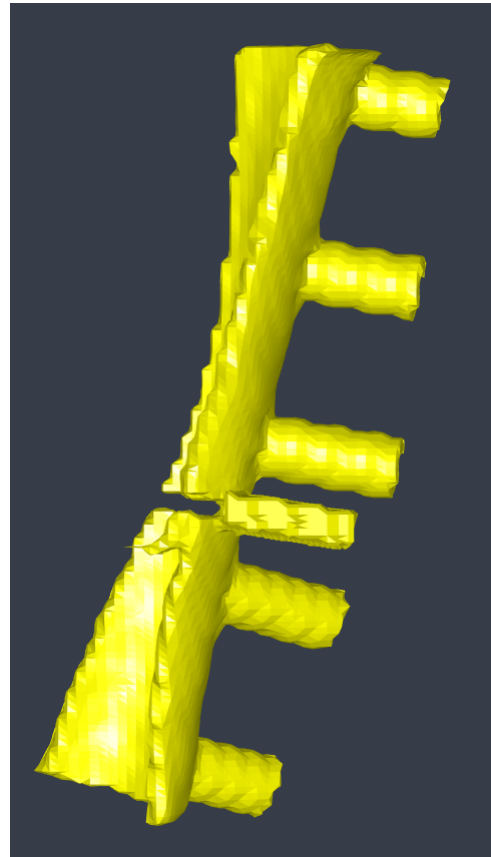
(a) Anterior view.

(b) Medial view.

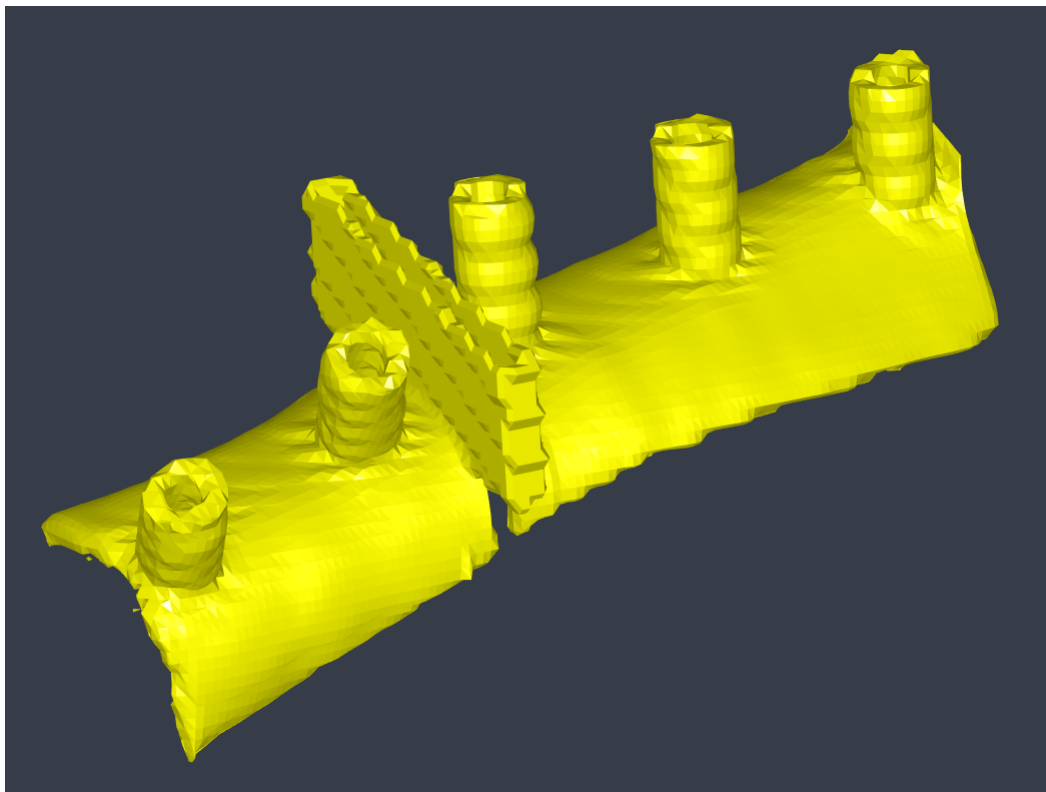
Figure B.4: Patient B plate placement (right radius malunion).



(a) Anterior view.



(b) Medial view.



(c) Anterolateral view.

Figure B.5: Patient B cutting guide (right radius malunion).

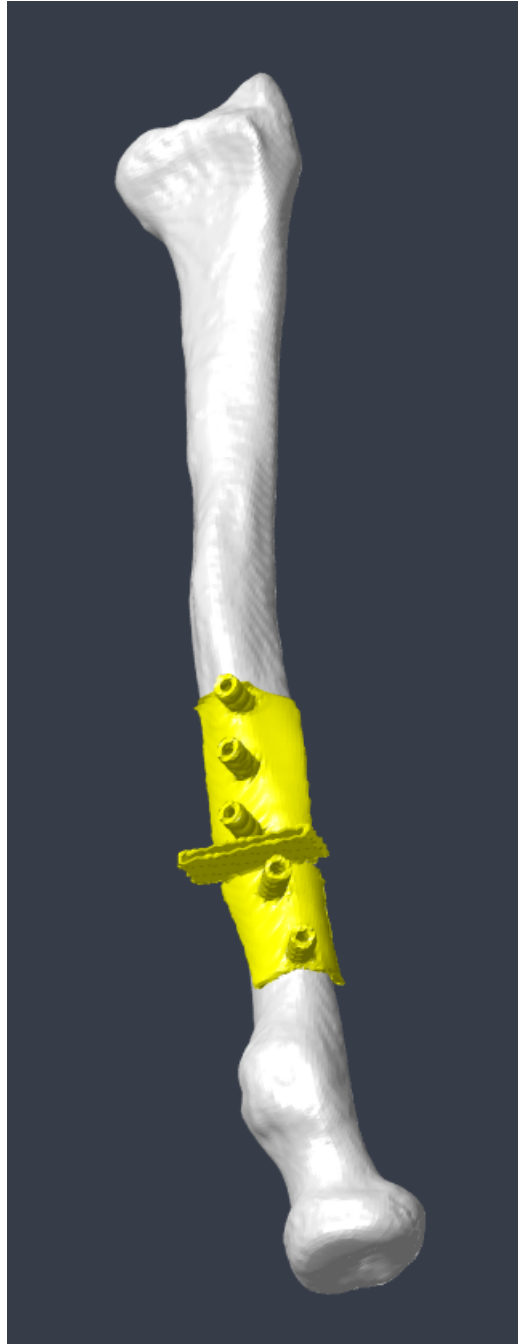


Figure B.6: Patient B cutting guide placement on deformed right radius.

Appendix C

Populärvetenskaplig sammanfattning

En fraktur på underarmen är väldigt vanligt och ibland blir det fel under läkningsprocessen. Då kan benet bli deformerat och orsaka stora problem för den drabbade och man behöver korrigera med en operation. Det här projektet tar fram ett hjälpmedel för kirurgen som både kortar ner operationstiden och som förbättrar operationsresultatet för patienten.

Underarmen består av två rörben, strålbenet (radius) och armbågsbenet (ulna), se figur C.1. Radius ledar mot överarmsbenet och ulna i armbågen och mot karpalbenen i handleden. Handleden är en s.k. äggled vilket gör att handleden dels kan böja och sträcka ut handen, dels röra handen i sidled.

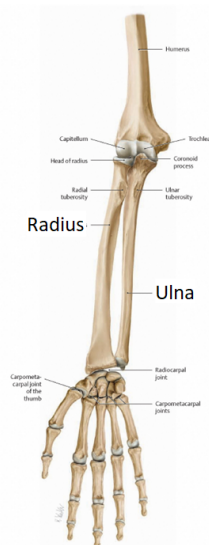


Figure C.1: Högra underarmens anatomi, radius and ulna.
Källa: Atlas of Anatomy Image Collection, Thieme Publishing Group.

En underarmsfraktur där antingen radius, ulna eller båda två är involverade är som sagt väldigt vanligt. Oftast uppstår frakturen nära handleden till följd av fall där man tar emot med handen. Dessa frakturer läker för det mesta fint med gipsning men ibland uppstår en deformation. Blir radius deformerat kan detta ge upphov till en felställning av benet och påverka ledytan i handleden. Detta kan orsaka smärta för patienten och även ge försämrad greppstyrka och rörelseförmåga.

En felställning kan behöva korrigeras med en operation. Då sågar kirurgen i benet, rätar upp det och fixerar med en metallplatta. Detta görs oftast på fri hand av kirurgen efter planering utifrån röntgenbilder. Ibland är dock felställningen så grov att det är svårt att avgöra var och hur man ska såga för att kunna räta upp benet och få det anatomiskt korrekt. För dessa fall kan man behöva använda en kapmall som sätts fast på det felställda radiusbenet under operationen. Kapmallen visar kirurgen exakt var sågningen ska göras och hur hålen för fixeringsplattan ska borraras för att få ett anatomiskt korrekt utseende på det rekonstruerade benet. En sådan kapmall

är specifik för patienten och beställs från specialiserade företag utomlands. Det är en mycket dyr service vilket tyvärr leder till att kapmallar används i mycket begränsad omfattning inom den svenska sjukvården.

Det här examensarbetet vill ändra på det och göra patientspecifika kapmallar mer lättillgängliga inom sjukvården. Med rekonstruktionsplanering och tillverkning av patientspecifika kapmallar på plats på Universitetssjukhuset i Lund skulle detta ge möjlighet för fler patienter att kunna opereras med en kapmall. Det gör operationerna både mer tidseffektiva och ökar chanserna att uppnå lyckade resultat.

För att uppnå detta så har ett program utvecklats där man i 3D kan planera en rekonstruktion av ett felställt radiusben. Programmet använder sig av en speglad version av patientens friska radiusben, vilket ger en referens för hur den felställda sidan bör se ut. I programmet kan man såga i benet och passa in ändarna så att dessa stämmer i ledytorna i armbågen och handleden. När man har gjort det kan man placera en fixeringsplatta över sågningen och rekonstruktionen är klar. Programmet flyttar

därefter tillbaka ändringarna och översätter dessa till en kapmall som passar exakt till det felställda benets utseende. Kapmallen kommer då ha en sågslits som visar hur sågningen ska göras och borrguider som visar var och hur man ska borra för att metallplattan ska fixera benet i rätt position, se figur C.2.

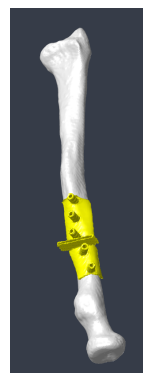


Figure C.2: Kap- och borrmall med passning för felställt radiusben.

Programmet testades på tre komplicerade patientfall och det togs fram en patientspecifik modell av en kapmall för vardera patient. Resultaten var lovande men det behövs en vidareutveckling av programmet och en utvärdering av kapmallarna för att kunna börja använda programmet för klinisk rekonstruktionsplanering.